

1 **Improving Madden–Julian Oscillation Simulation in Atmospheric General**
2 **Circulation Models by Coupling with Snow–Ice–Thermocline One-dimensional**
3 **Ocean Model**

格式化: 不要貼齊格線

4 Wan-Ling Tseng^{1,2}, Huang-Hsiung Hsu¹Hsu^{2*}, Yung-Yao Lan¹Lan², Wei-Liang Lee²,
5 Chia-Ying Tu¹Tu², Pei-Hsuan Kuo²Kuo³, Ben-Jei Tsuang³Tsuang⁴, Hsin-Chien
6 Liang¹Liang²

格式化: 靠左, 不要貼齊格線

格式化: 上標

7
8 ¹Research¹International Degree Program in Climate Change and Sustainable
9 Development, National Taiwan University, Taipei, Taiwan

格式化: 不要貼齊格線

10 ²Research Center for Environmental Changes, Academia Sinica, Taipei, Taiwan

格式化: 不要貼齊格線

11 ³Center³Center Weather Bureau, Taipei, Taiwan.

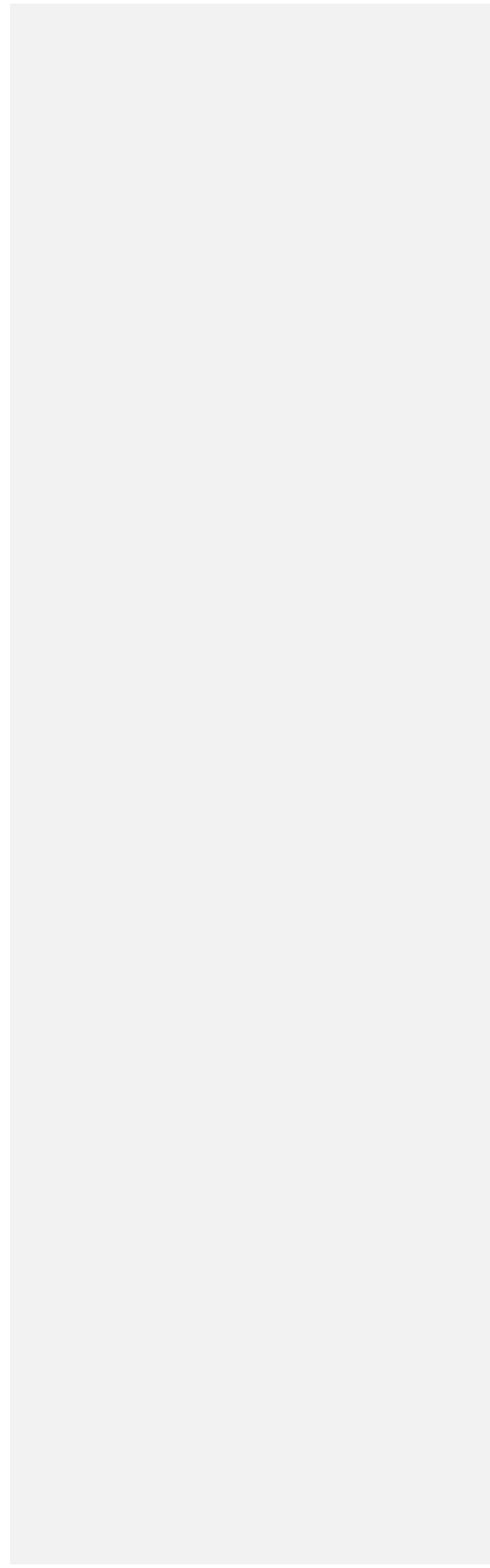
12 ⁴National⁴National Chung-Hsing University, Taichung, Taiwan.

13 Corresponding author: Huang-Hsiung Hsu (hhhsu@gate.sinica.edu.tw)

15 Abstract

16 A one-column turbulent kinetic energy--type ocean mixed-layer model ~~Snow-Ice-~~
17 ~~Thermoclinesnow-ice-thermocline~~ (SIT) when coupled with three atmospheric general
18 circulation models (AGCMs) ~~to yieldedyield~~ superior Madden-Julian Oscillation (MJO)
19 simulation. SIT is designed to have fine layers similar to those observed near the ocean
20 surface ~~and~~; therefore, it can realistically simulate the diurnal warm layer and cool skin.
21 This refined discretization of the near ocean surface in SIT provides accurate sea surface
22 temperature (SST) simulation; thus, facilitating realistic air-sea interaction. Coupling
23 SIT with European Centre Hamburg Model, Version 5-~~(ECHAM5)~~; Community
24 Atmosphere Model, Version 5-~~(CAM5)~~; ~~and~~ High-Resolution Atmospheric Model
25 ~~(HIRAM)~~ significantly improved MJO simulation in three coupled AGCMs compared
26 with the AGCM driven with prescribed SST. This study suggests two major
27 improvements to the coupling process. First, during the preconditioning phase of MJO
28 over the Maritime Continent (MC), the over underestimated surface latent heat bias in
29 AGCMs can be corrected. Second, during the phase of strongest convection over MC, the
30 change ~~of thein~~ intraseasonal circulation in the meridional circulation enhancing near-
31 surface moisture convergence is the dominant factor in the coupled simulations relative
32 to the uncoupled experiments. The study results ~~indicateshow~~ that a fine vertical
33 resolution near the surface, which better captures temperature variations in the upper few
34 meters of the ocean, considerably improves different models with different configurations
35 and physical parameterization schemes; this could be an essential factor for accurate MJO
36 simulation.

37 **Keywords:** Madden-Julian Oscillation, coupling, warm layer



39 **Short summary (plain text)**

40 We show that coupling a high-resolution one-column ocean model to three
41 atmospheric general circulation models dramatically improves Madden-Julian
42 ~~oscillation~~Oscillation (MJO) simulations. It suggests two major improvements to the
43 coupling process in the preconditioning ~~phase~~ and strongest convection ~~phase~~phases over
44 the Maritime Continent. Our results demonstrate a simple but effective way to
45 significantly improve MJO simulation and potentially ~~also~~-seasonal to subseasonal
46 prediction.

47

48

格式化: 不要貼齊格線

格式化: 行距: 2 倍行高, 不要貼齊格線

格式化: 不要貼齊格線

49 1 Introduction

50 The Madden–Julian Oscillation (MJO) is the dominant pattern of atmospheric
 51 intraseasonal variability in the tropics (Madden and Julian 1972; Zhang 2005; Jiang et al.
 52 2020)(Madden and Julian, 1972; Zhang, 2005; Jiang et al., 2020). It has been reported
 53 that the MJO convection is most often observed over sea surface temperature (SST) of
 54 >greater than 28°C in the Indo-Pacific warm pool (Salby and Hendon 1994). The (Salby
 55 and Hendon, 1994), MJO is an eastward-propagating ocean–atmosphere and convection–
 56 -circulation coupled phenomenon that lasts for 20–100 days. On these timescales, low-
 57 level moisture convergence, warm SST, and shallow upper-ocean mixed-layer depth
 58 precede the eastward propagation of organized deep convection by approximately 10ten
 59 days; opposite conditions followfollowed by approximately 10ten days (Krishnamurti et
 60 al. 1988; Hendon and Salby 1994; Woolnough et al. 2000)(Krishnamurti et al., 1988;
 61 Hendon and Salby, 1994; Woolnough et al., 2000). Heat flux exchange between the
 62 atmosphere and ocean modulates the intraseasonal oscillation (Shinoda and Hendon 1998;
 63 Shinoda et al. 1998). Studies have emphasized the importance of moisture and heat flux
 64 feedback in MJO. Heat flux exchange between the atmosphere and ocean modulates the
 65 intraseasonal oscillation (Shinoda and Hendon, 1998). Studies have emphasized the
 66 importance of moisture and heat flux feedback in MJO (Sobel et al. 2008, 2010; DeMott
 67 et al. 2015)(Sobel et al., 2008, 2010; DeMott et al., 2015). Besides, the MJO and oceanic
 68 wave dynamics are also suggested such as zonal wind stress anomalies associated with
 69 the MJO force eastward propagating oceanic equatorial Kelvin wave (Hendon et al. 1998;
 70 Webber et al. 2010), and the signals could extend as deep as 1500 m in the ocean
 71 (Matthews et al. 2007). Furthermore, the westward propagating oceanic equatorial
 72 Rossby wave can initiate the next MJO in the Indian Ocean (Webber et al. 2010; Webber

格式化: 字型色彩: 自動

格式化: 字型色彩: 自動

格式化: 字型色彩: 自動

格式化: 字型色彩: 自動

格式化: 字型色彩: 自動

格式化: 字型色彩: 自動

格式化: 字型色彩: 自動

格式化: 字型色彩: 自動

格式化: 字型色彩: 自動

格式化: 字型色彩: 自動

格式化: 字型色彩: 自動

73 ~~et al. 2012). Evidence of oceanic intraseasonal signals coupling with atmospheric signals~~
 74 ~~was observed in terms of the sea level, surface heat flux, salinity, and temperature during~~
 75 ~~field experiments and in situ monitoring. Besides, oceanic wave dynamics are suggested~~
 76 ~~to be associated with MJO, for example, zonal wind stress anomalies driven by the MJO~~
 77 ~~force eastward-propagating oceanic equatorial Kelvin wave (Hendon et al., 1998; Webber~~
 78 ~~et al., 2010), and the signals could extend as deep as 1500 m in the ocean (Matthews et~~
 79 ~~al., 2007). Furthermore, the westward-propagating oceanic equatorial Rossby wave can~~
 80 ~~initiate the next MJO in the Indian Ocean (Webber et al., 2010; Webber et al., 2012).~~
 81 ~~Evidence of oceanic intraseasonal signals coupling with atmospheric signals was~~
 82 ~~observed in terms of the sea level, surface heat flux, salinity, and temperature during field~~
 83 ~~experiments and in situ monitoring (Oliver and Thompson 2011; Drushka et al. 2012;~~
 84 ~~Wang et al. 2013; Chi et al. 2014; DeMott et al. 2015; Fu et al. 2015)(Oliver and~~
 85 ~~Thompson, 2011; Drushka et al., 2012; Wang et al., 2013; Chi et al., 2014; Matthews et~~
 86 ~~al., 2014; DeMott et al., 2015; Fu et al., 2015).~~

87 Recent modeling studies ~~evaluating the mechanism of ocean-atmosphere coupling~~
 88 have ~~indicated~~demonstrated that most coupled models could improve MJO simulations
 89 but that the ocean driven by the atmosphere contributes indirectly ~~through improvement~~
 90 ~~in~~by improving the mean state, heat flux, fresh water, and momentum. ~~DeMott et al.~~
 91 ~~(2016)~~DeMott et al. (2016) estimated that direct SST-driven ocean feedback contributes
 92 to the MJO propagation up to 10% by a change in column moisture. A comparison of the
 93 direct and indirect effects of SST indicated that direct effects, such as SST-driven surface
 94 fluxes, tend to offset wind-driven fluxes (~~DeMott et al. 2015; DeMott et al. 2016; DeMott~~
 95 ~~et al. 2019)~~(DeMott et al., 2015; DeMott et al., 2016; DeMott et al., 2019). The key-factor
 96 of indirect ocean feedback ~~in~~on the atmospheric physical process, ~~such as~~ includes strong

97 MJO convection can amplify the radiative feedback to MJO convections associated with
98 large cloud ~~systems~~ (Del Genio and Chen 2015), ~~the~~ (Del Genio and Chen, 2015).
99 ~~The~~ SST gradients can dive the MJO low-level convergence (Hsu and Li 2012; Li and
100 ~~Carbone 2012~~), ~~or~~ (Hsu and Li, 2012; Li and Carbone, 2012) and destabilize lower
101 tropospheric to further enhance low-level convergence to the east of MJO convergence
102 (~~Wang and Xie 1998; Marshall et al. 2008; Benedict and Randall 2011; Fu et al.~~
103 ~~2015~~) (Wang and Xie, 1998; Marshall et al., 2008; Benedict and Randall, 2011; Fu et al.,
104 ~~2015~~). Many observational and model studies have reported that coupled feedback
105 enhances the MJO with strong horizontal moisture advection, driven by sharp mean near-
106 equatorial meridional moisture gradients (~~DeMott et al. 2015; Jiang et al. 2018; DeMott~~
107 ~~et al. 2019; Jiang et al. 2020~~) (DeMott et al., 2015; Jiang et al., 2018; DeMott et al., 2019;
108 ~~Jiang et al., 2020~~). These ~~finding~~ findings suggest that high-frequency SST perturbations
109 could improve moisture convergence efficiency and enhance MJO propagation through
110 relatively smooth background moisture distribution.

111 ~~Tseng et al. (2015) identified the key role of the upper ocean warm layer in~~
112 ~~improving the MJO eastward propagation simulation by using the European Centre~~
113 ~~Hamburg Model, Version 5 (ECHAM5), coupled with the one-column ocean model~~
114 ~~named Snow-Ice-Thermocline (SIT). Many observational (Drushka et al. 2012; Chi et~~
115 ~~al. 2014) and modeling (Tseng et al. (2015) identified the key role of the upper-ocean~~
116 ~~warm layer in improving the MJO eastward propagation simulation using the European~~
117 ~~Centre Hamburg Model, Version 5 (ECHAM5), coupled with the one-column ocean~~
118 ~~model named snow-ice-thermocline (SIT). Many observational (Drushka et al., 2012;~~
119 ~~Chi et al., 2014) and modeling (Klingaman and Woolnough 2013; DeMott et al. 2019;~~
120 ~~Klingaman and Demott 2020)~~ (Klingaman and Woolnough, 2013; DeMott et al., 2019;

121 Klingaman and Demott, 2020 studies have supported this hypothesis. However, coupling
 122 the SIT to only one atmospheric general circulation model (AGCM) may be insufficient
 123 to prove the ~~effect~~effectiveness of the coupling. In ~~the current~~this study, we coupled the
 124 SIT to three AGCMs: ~~European Centre Hamburg Model, Version 5 (ECHAM5);~~
 125 Community Atmosphere Model, Version 5 (CAM5);~~;~~ and High-Resolution
 126 Atmospheric Model (HiRAM). ~~As well as one additional high resolution forecast model~~
 127 ~~from Central Weather Bureau, Taiwan (CWBGFS) to demonstrate that the improvement~~
 128 ~~of MJO simulation through coupling the upper ocean warm layer is AGCM independent.~~
 129 ~~Furthermore, we~~We also discussed the coupling mechanism that leads to simulation
 130 improvement. ~~Models, the~~

131 The remainder of the paper is organized as follows. In section 2, we describe the
 132 models, experimental designs, and observational data are described in Section 2.
 133 Section 3 presents and 4 present the results, ~~followed by a and~~ discussion ~~in Section 4.~~
 134 respectively.

135 **2 Models, Data, model experiments, and observational methodology**

136 **2.1 Observation and atmospheric/oceanic data**

137 ~~Observational data used in this study include precipitation from Global Precipitation~~
 138 ~~Climatology Project V1.3 (GPCP, 1° resolution) (Adler et al. (2003), outgoing longwave~~
 139 ~~radiation (OLR, 1° resolution) (Liebmann (1996)), and daily SST (Optimum Interpolated~~
 140 ~~SST, 0.25° resolution) (Banzon et al. (2014)) from the National Oceanic and Atmosphere~~
 141 ~~Administration, and variables were obtained from the European Centre for Medium-range~~
 142 ~~Weather Forecast Reanalysis interim (Dee et al. 2011). We used a 22-year ERA Interim~~

格式化: 不要貼齊格線

格式化: 字型色彩: 自動

格式化: 字型色彩: 自動

格式化: 字型色彩: 自動

格式化: 字型色彩: 自動

格式化: 字型色彩: 自動

格式化: 字型色彩: 自動

格式化: 內文, 縮排: 第一行: 0.63 公分, 行距: 單行間距, 不要貼齊格線

143 from 1989 to 2010 and a 14-year GPCP dataset from 1997 to 2010. Oceanic observational
144 data include those from the NCEP Global Ocean Data Assimilation System (GODAS)
145 (Behringer and Xue (2004) provided by the NOAA/OAR/ESRL PSL, Boulder, Colorado,
146 USA (<https://psl.noaa.gov/data/gridded/data.godas.html>) and in-situ temperature profiles
147 from the Tropical Ocean Global Atmosphere program (McPhaden et al. 2010).

148 In this study, we coupled the SIT one-column ocean model (Tu and Tsuang 2005;
149 Tsuang et al. 2009) to four AGCMs. SIT simulates variations in the SST and upper ocean
150 temperature, including the diurnally varying cool skin and warm layer in the upper few
151 meters of the ocean and the turbulent kinetic energy (TKE) (Gaspar et al. (1990)) in the
152 water column. Observational data used in this study include precipitation from Global
153 Precipitation Climatology Project V1.3 (GPCP, 1° resolution, 1997–2010; Adler et al.,
154 2003), outgoing longwave radiation (OLR, 1° resolution, 1997–2010; Liebmann, 1996)
155 and daily SST (Optimum Interpolated SST, 0.25° resolution, 1989–2010; Banzon et al.,
156 2014) from the National Oceanic Atmosphere Administration. The in situ ocean
157 temperature profiles from 1989 to 2010 were obtained from the Tropical Ocean Global
158 Atmosphere program (McPhaden et al., 2010).

159 Atmospheric variables were obtained from the European Centre for Medium-range
160 Weather Forecast Reanalysis-interim (Dee et al., 2011) from 1989 to 2010. The variables
161 include zonal wind, meridional wind, temperature, specific humidity, sea level pressure,
162 geopotential high, latent heat, sensible heat, shortwave and longwave radiation. Oceanic
163 temperature data from 1989 to 2010 were obtained from the NCEP Global Ocean Data
164 Assimilation System (GODAS) (Behringer and Xue, 2004) provided by the
165 NOAA/OAR/ESRL PSL, Boulder, Colorado, USA
166 (<https://psl.noaa.gov/data/gridded/data.godas.html>).

2.2 Model experiments

In this study, we coupled the one-column ocean model SIT (Tu and Tsuang, 2005; Tsuang et al., 2009) to three AGCMs. SIT simulates variations in the SST and upper-ocean temperature, including the diurnally-varying cool skin and warm layer in the upper few meters of the ocean and the turbulent kinetic energy (TKE; Gaspar et al., 1990) in the water column (Tu and Tsuang 2005; Tsuang et al. 2009; Tseng et al. 2015) (Tsuang et al., 2001; Tu and Tsuang, 2005; Tu, 2006; Tsuang et al., 2009; Tu and Tsuang, 2014; Tseng et al., 2015; Lan et al., 2021). The four AGCMs used here are as follows. (1) ECHAM5, a the fifth generation AGCM developed at the Max Planck Institute for Meteorology (Roeckner 2003; Roeckner et al. 2006). It is a spectral model employing the Nordeng (Nordeng 1994) cumulus convective scheme. We used a horizontal resolution of T63 (approximately 2°) with 31 vertical layers and a model top at 10 hPa (approximately 30 km). (2) NCAR CAM5 in Community Earth System Model, version 4.2.2 (Hurrell et al. 2013) from the National Center for Atmospheric Research. (3) HiRAM, developed based on Geophysical Fluid Dynamical Laboratory global atmosphere and land model AM2 (Team et al. 2004; Zhao et al. 2009) with few modifications (Chen et al. 2019). We also used CWBGFS, the second generation global forecast system at the Central Weather Bureau in Taiwan (Liou et al. 1997), which employs the cumulus convective scheme of Nordeng (1994), shallow convective scheme of (Li and Wang 2000), and boundary layer of Hong and Pan (1996).

In this study, we applied. Cool skin is a very thin layer that has a direct contact with the atmosphere and warm layer is the warmer sea water immediately below the cool skin in the top few meters of the ocean. They fluctuate diurnally in response to atmospheric forcing. SIT with high vertical resolution realistically simulates the warm-layer (within

191 top 10 m) and cool-skin (the top layer with 0.001 m thickness), and improve the
 192 simulation of upper ocean temperature (Tu and Tsuang, 2005; Tsuang et al., 2009). The
 193 model has been verified at a tropical ocean site (Tu and Tsuang, 2005), in the South China
 194 Sea (Lan et al., 2010), and Caspian Sea (Tsuang et al., 2001). The melt and formation of
 195 snow and ice above a water column have been introduced (Tsuang et al., 2001). The three
 196 AGCMs used in this study are as follows. ECHAM5, the fifth-generation AGCM
 197 developed at the Max Planck Institute for Meteorology (Roeckner, 2003; Roeckner et al.,
 198 2006) is a spectral model that employs the Nordeng (Nordeng, 1994) cumulus convective
 199 scheme. We used a horizontal resolution of T63 (approximately 2°) with 31 vertical layers
 200 and a model top at 10 hPa (approximately 30 km). The second one is NCAR Community
 201 Atmospheric Model version 5 (Hurrell et al., 2013) from the National Center for
 202 Atmospheric Research. We used a horizontal resolution of approximately
 203 1.875° latitude × 2.5° longitude and 30 vertical layers with the Zhang–McFarlane
 204 deterministic convection scheme (Zhang and McFarlane, 1995) and the University of
 205 Washington Shallow Convection (Park and Bretherton, 2009). HiRAM was developed
 206 based on Geophysical Fluid Dynamical Laboratory global atmosphere and land model
 207 AM2 (Team et al., 2004; Zhao et al., 2009) with few modifications (Chen et al., 2019).
 208 We used a horizontal resolution of 0.5° latitude × 0.5° longitude with 32 vertical levels.
 209 For boundary layer and free atmospheric turbulence, the model adopted the 2.5 order
 210 parameterization of Mellor and Yamada (1982). Surface fluxes are computed based on
 211 the Monin–Obukhov similarity theory, given the atmospheric model’s lowest level of
 212 wind, temperature, and moisture.

213 There are 42 vertical layers in SIT, with 12 layers in the upper 10 m. In the upper 10
 214 m: the surface, 0.05 mm, 1 m, 2 m, 3 m, 4 m, 5 m, 6 m, 7 m, 8 m, 9 m, and 10 m below

格式化: 不要貼齊格線

215 ocean surface. The fine resolution was designed to realistically simulate the upper-ocean
216 warm layer, including a layer at 0.05 mm, reproducing the cool skin of the ocean surface.
217 ~~Notably, it is worth noting that~~ coupling of a high-vertical-resolution TKE ocean model
218 with an AGCM is unconventional. To account for neglected horizontal processes, the
219 model ocean was weakly nudged (with a 30-day time scale) to the observed GODAS
220 monthly mean ocean temperature below a depth of 10 m. Nudging was not applied in the
221 upper 10 m. The timestep of SIT and AGCMs exchange ocean surface fluxes ~~at every~~
222 ~~time step 48 times a day~~ varying associated with the model resolution, which is 720, 1800,
223 and 900 seconds in ECHAM-SIT, CAM5-SIT, and HiRAM-SIT, respectively. AGCMs
224 were coupled with the SIT in the tropical region between 30°S and 30°N and forced by
225 prescribed ~~climatological~~ monthly mean SSTOISST outside this tropical belt.

226 The experiments ~~included~~ comprised three sets of coupled AGCM simulations
227 (ECHAM5-SIT, CAM5-SIT, and HiRAM-SIT) and standalone AGCM simulations
228 forced by observed monthly mean OISST (ECHAM5, CAM5, and HiRAM) from 1985
229 to 2005. The experiments were designed to evaluate the effect of atmosphere–ocean
230 coupling on MJO simulations. Table 1 presents the model and experiment details. ~~Due to~~
231 ~~the computation limitation of a high-resolution forecast model, the CWBGFS SIT was~~
232 ~~only run for 3 years to test the coupling effect. Thus, its results were evaluated but not~~
233 ~~compared with those of the other three models.~~

234 ~~The analysis focused on the boreal cool season (November–April) when the eastward~~
235 ~~propagation tendency of the MJO is the most prominent. We used the CLIVAR MJO~~
236 ~~Working Group diagnostics package (CLIVAR 2009) and a 20–100-day filter to analyze~~
237 ~~intraseasonal variability. The MJO phase composites were computed using the real-time~~
238 ~~multivariate MJO index (Wheeler and Hendon 2004), which is defined as the leading pair~~

of principal components of intraseasonal OLR, and 850 and 200 hPa zonal winds in the tropics.

2.3 Methodology

The analysis focused on the boreal cool season (November–April) when the eastward propagation tendency of the MJO is the most prominent. We used the CLIVAR MJO Working Group diagnostics package (CLIVAR, 2009) and a 20–100-day filter to analyze intraseasonal variability. The MJO phase composites were computed using the real-time multivariate MJO index (Wheeler and Hendon, 2004), defined as the leading pair of principal components of intraseasonal OLR, and 850 and 200 hPa zonal winds in the tropics.

The vertically integrated MSE budget was diagnosed based on the following equation:

$$\left\langle \frac{\partial h}{\partial t} \right\rangle = - \left\langle u \frac{\partial h}{\partial x} \right\rangle - \left\langle v \frac{\partial h}{\partial y} \right\rangle - \left\langle \omega \frac{\partial h}{\partial p} \right\rangle + \langle LW \rangle + \langle SW \rangle + \langle LH \rangle + \langle SH \rangle \quad (1)$$

where h is the MSE ($h = cpT + gz + Lq$); u and v are the zonal and meridional velocities, respectively; ω is the vertical pressure velocity; LW and SW are the longwave and shortwave radiation fluxes, respectively; LH and SH are the latent and sensible surface heat fluxes, respectively. The mass-weighted vertical integration from the surface to 200 hPa is denoted as $\langle \cdot \rangle$, and intraseasonal anomalies are represented as $\langle \cdot \rangle'$. All fields, which were isolated using a 20–100-day bandpass Lanczos filter (Duchon 1979) (Duchon, 1979).

3 Results

3.1 MJO simulations: ECHAM5-SIT, CAM5-SIT, and HiRAM-SIT

格式化: 不要貼齊格線

261 3.1.1 General structure

262 We compared simulated MJO characteristics using three coupled and uncoupled
 263 AGCMs. Figure 1 ~~presents~~shows the wavenumber–frequency spectra of simulated 850–
 264 hPa zonal wind (shading) and precipitation (contours). All three uncoupled AGCMs
 265 (hereafter referred to as AGCMs) simulated intraseasonal signals with lower frequency
 266 than the observed and overestimated the westward propagation with periods >greater than
 267 80 days (~~FigFigs.~~ 1e–g). The ECHAM5 and HiRAM simulated signals of wavenumbers
 268 1–3 instead of the observed wavenumber 1 in 850–hPa zonal wind. These results
 269 ~~indicates~~show that all three AGCMs simulated stationary fluctuations with low frequency
 270 that were not consistent with the observation. By contrast, coupled AGCMs realistically
 271 reproduce the observed spectral characteristics and strength of the eastward propagation
 272 at wavenumbers 1 to 2 in 850-hPa zonal wind (~~FigFigs.~~ 1b–d). Although HiRAM
 273 simulated eastward propagation in a wider frequency spectrum than ~~that~~the observed, the
 274 coupled model clearly displays improvements in the MJO simulation compared with the
 275 stationary intraseasonal fluctuation in the uncoupled simulation. Hovmöller diagrams
 276 presented in Fig. 2 illustrate the temporal evolution of 850–hPa zonal wind and
 277 precipitation in the tropics in observation and simulations. All three models simulated
 278 either stationary (CAM5 and HiRAM) or weak eastward-propagating (ECHAM5) signals
 279 in AGCMs, but more realistically simulated the eastward propagation of the MJO in the
 280 ~~coupled AGCMs, although models. However,~~ the propagation in the ECHAM5-SIT is still
 281 slightly slower than ~~that~~the observed. The improvement obtained in coupled models
 282 suggests that active ocean–atmosphere interaction is ~~a~~-crucial ~~factor~~ for ~~the~~-successful
 283 MJO simulation ~~of the MJO~~.

284 3.1.2 Atmospheric and oceanic profiles

285 The composite MJO life cycle featuring intraseasonal OLR and 10-m surface wind
 286 anomalies for boreal winter in eight phases following ~~Wheeler and Hendon (2004) is~~
 287 ~~displayed in Fig. S1-S3. All three coupled AGCMs~~ Wheeler and Hendon (2004) is
 288 displayed in Fig. 3. All three coupled models simulated realistic MJO with enhanced
 289 circulations and propagation tendency compared with the uncoupled ~~AGCMs. Figure 3~~
 290 ~~shows the temporal evolution of vertical heating profiles (averaged over 10°S-EQ,~~
 291 ~~120°E-150°E) in eight MJO phases. Observed heating profiles, calculated following the~~
 292 ~~definition of the apparent heat source (Q1) (Yanai et al. 1973), exhibit diabatic heating~~
 293 ~~with a maximum near 500 hPa in phases 4 and 5 and in the lower troposphere in earlier~~
 294 ~~phases. This reflects the development from shallow to deep heating during the~~
 295 ~~development stage of the convective phase in an MJO. Both ECHAM and HiRAM exhibit~~
 296 ~~stronger heating in coupled simulations than in uncoupled simulations, whereas the~~
 297 ~~difference is not evident in CAM5. The vertical structures of the apparent moisture sink~~
 298 ~~(Q2; contours) associated with the MJO demonstrate a similar convection development.~~

299 MJO analysis in phase 4 when deep convection is the strongest over the Maritime
 300 Continentalones. The MJO in phase 4, when deep convection is the strongest over the
 301 Maritime Continent (MC), demonstrates the large-scale zonally overturning circulation
 302 coupling with the convection (Fig. 4). The positive heating region in the coupled
 303 experiment is significantly enlarged, deepened, and westward-tilted with increasing
 304 height compared with those in the uncoupled experiment. Correspondingly, the
 305 convective-circulation envelope of the MJO is thicker and longitudinally wider in coupled
 306 experiments. The strong convection is associated with much enhanced low-level moisture
 307 convergence (green contours). Furthermore, the area of positive rainfall anomaly in the
 308 coupled experiment becomes larger, and the sea level pressure anomaly is meridionally

格式化: 不要貼齊格線

309 more confined, exhibiting the characteristics of intensified Kelvin wave-like
 310 perturbations to the east of the deep convection. This enhancement of low-level moisture
 311 convergence is consistent with the frictional wave—conditional instability of the second
 312 kind mechanism ~~(Wang and Rui 1990; Kang et al. 2013)~~(Wang and Rui, 1990; Kang et
 313 al., 2013). The enhancement of the Kelvin wave can be observed in the symmetric
 314 wavenumber–frequency spectra (Fig. 5). The spectra between 0 and 0.35 day⁻¹ are
 315 presented to highlight the MJO and equatorial Kelvin waves. The coherence at
 316 wavenumbers of 2–4 for the 10–20-day period is simulated stronger in three coupled than
 317 uncoupled models.

318 In addition to the atmospheric structure, the SST (Fig. ~~S4S1~~) and vertical profile of
 319 ocean temperature ~~(Fig. S5)~~ examined are presented in Fig. ~~S56~~. The observed SST
 320 variation in MJO variability is well reproduced in all three coupled models (Fig. ~~S4S1~~).
 321 The warm SST leads the main MJO convection by approximately 5–10 days ~~and is,~~
 322 followed by the cold SST approximately 5–10 days later ~~(Flatau et al. 1997; DeMott et~~
 323 ~~al. 2015; Tseng et al. 2015)~~(Flatau et al., 1997; DeMott et al., 2015; Tseng et al., 2015).
 324 Moreover, the observed amplitude fluctuation (approximately 0.5° to 1°C) is realistically
 325 simulated. ~~Observed~~The observed ocean temperature profiles, characterized by the warm
 326 layer, along the equator from the Indian Ocean to the western Pacific are well simulated
 327 in the three coupled models (Fig. ~~S5~~). ~~Simulated temperature anomalies are larger in~~
 328 ~~ECHAM5-SIT than in CAM5-SIT and HiRAM-SIT. These results consistently~~
 329 ~~obtained~~6). Meanwhile, simulated temperature anomalies are larger in ECHAM5-SIT
 330 than in CAM5-SIT and HiRAM-SIT. Figure. S2 shows the fluctuations of observed SST
 331 and simulated SST in three sets of coupled and uncoupled model. There is no fluctuation
 332 as expected in uncoupled simulations, whereas the simulated SST fluctuates with phases

333 ~~similar to the observed at different locations. The amplitudes in ECHAM5-SIT and~~
 334 ~~CAM5-SIT are similar to the observed, whereas those in HiRAM-SIT seems to be smaller~~
 335 ~~in the western Pacific. The differences between models are likely due to the different~~
 336 ~~atmospheric model configurations, because they were coupled to the same 1-D ocean~~
 337 ~~model. Since the atmosphere is the main driver to extract heat form the ocean, different~~
 338 ~~responses of atmospheric models likely have different effects on SST. The cause of~~
 339 ~~quantitative differences between models needs further detailed analysis to pinpoint. The~~
 340 ~~consistent results~~ in all three coupled models support the conclusion of Tseng et al. (2015)
 341 that resolving fine vertical resolution in the upper ocean improves the simulation of ~~the~~
 342 warm layer and MJO propagation and variability. ~~The Our results further demonstrate~~
 343 ~~that the~~ effect of atmosphere–ocean coupling on the MJO ~~is could be~~ independent of
 344 AGCMs with different configurations and atmospheric physical parameterizations.
 345 ~~Modifying atmospheric physical parameterizations has been shown to improve MJO~~
 346 ~~simulation to some extent (Wang et al. 2021), and the results could be model dependent.~~
 347 ~~Our results demonstrate that the impact of atmosphere–ocean that coupling independent~~
 348 ~~of physical schemes~~ seems to be a more fundamental approach.

349 3.1.3 Performance comparison

350 ~~To summarize improvements resulting from coupling, simulation was evaluated~~
 351 ~~(Model performance is summarized in Fig. 5). Figure 5a presents the~~7. The scatter plot
 352 ~~of shows~~ the power ratio of east–west propagating waves (X-axis) versus the pattern
 353 correlation between the simulated and observed precipitation anomaly in Hovmöller
 354 diagrams (Fig. 2) ~~(Y-axis)~~. The east:west ratio was calculated by dividing eastward-
 355 propagating power by westward-propagating power of 850–hPa zonal wind summed

格式化: 行距: 2 倍行高, 不要貼齊格線

356 over wavenumbers of 1–2 and a period of 30–80 days. Compared with the observation,
 357 coupled simulations (marked by circles) exhibit better simulation than uncoupled
 358 simulations (marked by asterisks). A comparison of combined explained variance by
 359 using RMM1 and RMM2 (Fig. 5b7b) based on Wheeler and Hendon (2004) shows
 360 marked increases after coupling. AThe comparison of the coupled and uncoupled
 361 simulations demonstrates that coupling is an essential factor for realistic MJO simulations.

362 3.2 Mechanism discussion

363 Here, We applied the MSE budget was applied to diagnose the moisture budget
 364 associated with the MJO. Figure 6 presents8 shows a Hovmöller diagram of MSE
 365 tendency averaged by 10°S–EQ overlaying precipitation anomalies. MSE tendency
 366 changes derived from reanalysis fluctuates in quadrature with precipitation anomaly with
 367 positive (negative) MSE tendency, leading (lagging) major convection by approximately
 368 one to two phases (DeMott et al. 2015; DeMott et al. 2016; DeMott et al. 2019)(DeMott
 369 et al., 2015; DeMott et al., 2016; DeMott et al., 2019). Coupled models simulate stronger
 370 eastward propagation in both the MSE tendency and precipitation anomalies. and realistic
 371 phase lag between the two. Stronger MSE tendencies in coupled simulations are
 372 seen observed in ECHAM5 and HiRAM but are less clear in CAM5. The Figures 8d, g,
 373 and j show the differences between coupled and uncoupled simulations are presented in
 374 Fig. 6d, g, j. One notable feature is the positive (negative) MSE tendency preceding
 375 positive (negative) precipitation anomaly and preconditions an environment for eastward
 376 propagation of active (inactive) convection and associated circulation. WeNext, we
 377 diagnosed the relative contribution of each term in Equation 1 to the MSE tendency with

格式化: 不要貼齊格線

378 the focus on the MC, where the largest positive MSE tendency and precipitation anomaly
 379 were found.

380 3.2.1 Preconditioning phase

381 Following the peak MSE tendency over the MC (120°E–150°E) during phase 2 (~~Fig.~~
 382 ~~6d~~~~Figs. 8d, g, and j~~), values of each term contributing to the column-integrated MSE
 383 tendency in Equation 1 ~~during phase 2~~ preceding the deep convection over the MC area
 384 (10°S–EQ, 120°E–150°E) are ~~displayed~~~~shown~~ in Fig. 79. Vertical advection is the
 385 dominant term with the major compensation from ~~long-wave~~~~longwave~~ radiation during
 386 phase 2 when convection is still in the eastern Indian Ocean, as identified by Wang et al.
 387 (2017). ~~However, this effect is not better simulated in the coupled experiments than in the~~
 388 ~~uncoupled experiments in all three models. Notably, the LH term is consistent between~~
 389 ~~both phases. In all three models, the coupling reduces the negative MSE tendency. The~~
 390 ~~results indicate that the contribution comes for the LH in this early phase stage. The LH~~
 391 ~~effect was overlooked in Tseng et al. (2015) because of the weak MJO variability in~~
 392 ~~coupled simulations. However, this smaller LH negative became~~~~Moreover, the LH term~~
 393 ~~is consistent within all three models to contribute less negative MSE tendency in coupled~~
 394 ~~models than ACGMs. The results show that the contribution comes from the LH term in~~
 395 ~~this early phase stage. The LH effect was overlooked in Tseng et al. (2015) because of~~
 396 ~~the weak MJO variability in coupled simulations. However, this negative LH bias~~
 397 ~~becomes~~ one of the key factors in enhancing the leading MSE tendency during the MJO
 398 preconditioning phases. This suggests that ~~the surface latent flux bias in AGCMs can be~~
 399 ~~corrected~~ by involving the coupling process in the preconditioning phase, ~~the surface~~
 400 ~~latent flux bias in AGCMs can be corrected. In general, Generally,~~ coupling improves the

401 ~~budget~~ simulation ~~of budget~~. The positive contribution of vertical advection and negative
 402 contribution of LH in MSE tendency is closer to realistic in the coupled simulations
 403 during the initial phase of the MJO.

404 3.2.2 Phase of strongest convection over MC

405 We compared the spatial distribution of MSE and precipitation in phase 4 when
 406 convection was the strongest in the MC (Fig. 810). In the observation, the main
 407 convection occurs in the MC from 90°E to 150°E. A positive MSE tendency with a
 408 maximum value near 10°N and 10°S is identified in the east of the MJO convection
 409 centered near the equator. ~~Conversely~~ ~~Meanwhile~~, a negative integrated MSE tendency is
 410 found in the west of the MJO convection, and the meridionally confined structure near
 411 the equator ~~seems to exhibit~~ exhibits the characteristics of the equatorial Kelvin wave
 412 embedded in the MJO. Clearly, coupled models outperform uncoupled models in
 413 reproducing these signals. To quantify the contribution of coupling to the improvement,
 414 we follow Jiang et al. (2018) to project all MSE terms to the observations (Fig. 9). ~~The~~
 415 ~~dominant contribution of horizontal advection to the MSE tendency in observation (Fig.~~
 416 ~~9a)~~ Jiang et al. (2018) to project all MSE terms to the observations (Fig. 11). ~~The dominant~~
 417 ~~contribution of horizontal advection to the MSE tendency in observation (Fig. 11a)~~ is well
 418 simulated in the coupled simulations but not in uncoupled simulations by ECHAM5 and
 419 CAM5 (~~Fig. 9b, Figs. 11b and c~~). Although a similar dominant effect ~~is noted~~ ~~was~~
 420 observed in both simulation types in HiRAM, it is ~~more~~ enhanced in the coupled
 421 simulation (Fig. ~~9d~~ 11d). The horizontal advection term is further decomposed into zonal
 422 and meridional components (~~Fig. 9e~~ Figs. 11e-h); both components have a positive
 423 contribution, but the meridional component has a larger amplitude.

格式化: 行距: 2 倍行高, 不要貼齊格線

424 ~~Uncoupled~~ Furthermore, the uncoupled ECHAM5 and CAM5 simulate unrealistic
 425 features: positive contribution from zonal advection but negative contribution from
 426 meridional advection. ~~By~~In contrast, coupled models well simulate the dominance of
 427 meridional advection. In HiRAM, the uncoupled model simulates almost equally positive
 428 contributions from both terms, ~~but~~ However, the coupled model ~~is able to simulate~~
 429 ~~thesimulates a~~ larger contribution from meridional advection. We further decompose the
 430 meridional advection to assess the relative contributions of ~~an~~ intraseasonal perturbation
 431 and the mean state. Consistent with the observations (Fig. 9; 11i), the meridional advection
 432 by intraseasonal flow ($-v' \frac{\partial \bar{h}}{\partial y}$) is the main ~~contribution to improve~~ factor in improving
 433 the simulations in the coupled models (Fig. 9; Figs. 11j–l). Our results are consistent with
 434 those of ~~Jiang et al. (2018)~~, Jiang et al. (2018). To evaluate the relative contribution of
 435 intraseasonal circulation and background moisture, ~~we further diagnosed~~ changes in
 436 $\Delta(-v' \frac{\partial \bar{h}}{\partial y})$ at phase 4 ~~were further diagnosed~~. ~~Overbar denotes~~. ~~Here the overbar shows~~
 437 that the time mean and prime represents intraseasonal anomaly. Changes in the MJO
 438 meridional advection term for coupled experiments relative to uncoupled can be written
 439 as follows:

$$440 \Delta\left(-v' \frac{\partial \bar{m}}{\partial y}\right) = -\Delta v' \left(\frac{\partial \bar{m}}{\partial y}\right)_{uncoupled} - \left(v'\right)_{uncoupled} \Delta\left(\frac{\partial \bar{m}}{\partial y}\right) - \Delta v' \Delta\left(\frac{\partial \bar{m}}{\partial y}\right) \quad (2)$$

441 (a) (b) (c)

442 where Δ represents the coupled–uncoupled change. The terms a–c are presented as bar
 443 charts in Fig. 10. ~~Notably, the~~ 12. The change of the intraseasonal circulation in the
 444 meridional circulation is the dominant factor in coupled simulations relative to uncoupled

格式化: 不要貼齊格線

格式化: 行距: 2 倍行高, 不要貼齊格線

445 experiments. The instantaneous SST horizontal distribution dominates this moisture
 446 budget change due to the atmosphere–ocean coupling effect. Therefore, the change of
 447 varying moisture induces the intraseasonal circulation change. The results confirm that
 448 the dominance of dynamic influence over thermodynamic response to atmosphere–ocean
 449 coupling is ~~the key process leading to an improvement in~~ essential in improving MJO
 450 simulations.

451

452 3.3 Discussion: mean state and intraseasonal variance

453 We examined the simulated mean state, which ~~is~~ has been suggested a major issue ~~key~~
 454 factor affecting MJO simulations (~~Inness et al. 2003; Watterson and Syktus 2007; Kim et~~
 455 ~~al. 2009; Kim et al. 2011; Kim et al. 2014; Jiang et al. 2018; Jiang et al. 2020~~) Inness et
 456 al., 2003; Watterson and Syktus, 2007; Kim et al., 2009; Kim et al., 2011; Kim et al.,
 457 2014; Jiang et al., 2018; Jiang et al., 2020). The three models exhibited different tropical
 458 SST responses to coupling (Fig. ~~S6e~~ S3e). Over the warm pool area, ~~both~~ CAM-SIT and
 459 HiRAM-SIT underestimate the SST, whereas ECHAM5-SIT overestimates the SST.
 460 ~~Warm~~ Note that warm SST bias in the eastern tropical Pacific was simulated in the three
 461 models ~~because of~~ due to the lack of oceanic circulation in the SIT. The simulated zonal
 462 wind in the three models (Fig. ~~S6b~~ Figs. S3b–d) demonstrated different responses to
 463 coupling. ~~Figure S6e, d presents~~ Figures S2c show the 850–hPa zonal wind differences
 464 between coupled and uncoupled models (shading) and the total field in uncoupled models
 465 (contours). ~~Figure S6f~~ Figures S3f–h show the 10°S–EQ averaged 850–hPa zonal
 466 wind in ~~both~~ the coupled and uncoupled models. In ECHAM5-SIT, the westerly wind is slightly
 467 enhanced in the eastern Indian Ocean but decreases in the western Indian Ocean and

468 western Pacific. In CAM5-SIT, westerly wind reduces in the Indian Ocean but enhances
 469 over the western Pacific. The HiRAM-SIT has similar changes as in ECHAM5-SIT,
 470 ~~with e.g.~~ decreases over the ~~Maritime Continent~~MC area but increases in the western
 471 Indian Ocean and Pacific. ~~In general~~Generally, the three models disagree ~~in~~on the
 472 ~~changes in~~ zonal wind mean state ~~changes~~ in response to coupling.

473 The mean moisture changes are substantially enhanced over the tropical areas in
 474 ECHAM5 after coupling (~~Fig. S7b, Figs. S4b and e~~). However, in ~~both~~ CAM5 and
 475 HiRAM, no clear change was observed to the south ~~of the equator~~, but strong drying was
 476 observed to ~~in~~ the north ~~of equator~~ (~~Fig. S7e~~(~~Figs. S4c, d, f, and g~~). The only common
 477 feature among the three models ~~that is the enhanced in the coupled simulations is the~~
 478 meridional gradient of mean moisture. ~~This, which~~ is consistent with many previous
 479 studies (~~Kim et al. 2014; Jiang et al. 2018; Ahn et al. 2020~~)(~~Kim et al., 2014; Jiang et al.,~~
 480 ~~2018; Ahn et al., 2020~~). Our budget analysis ~~indicated~~demonstrated that the meridional
 481 transport by the intraseasonal meridional circulation is the dominant term, ~~and. It also~~
 482 ~~showed that~~ the meridional gradient of mean moisture is the secondary effect in enhancing
 483 MJO simulations by coupling. ~~The~~After coupling, the mean precipitation changes are
 484 more consistent among the three models ~~after coupling~~ (Fig. ~~S8S5~~). One of the major
 485 changes is the southward shift of the major precipitation zone, resulting in precipitation
 486 increases over the regions south of the equator, except in the ~~Maritime Continent~~MC.
 487 Similarly, the precipitation intraseasonal variance (20–100 days filtered) ~~was~~ markedly
 488 ~~enhances~~enhanced in these regions (Fig. ~~S9S6~~). The ECHAM5-SIT exhibits a relatively
 489 minor increase over the western ~~Maritime Continent~~MC. ~~By~~MC. In contrast, the HiRAM-
 490 SIT exhibits the strongest enhancement, particularly in the Indian Ocean. ~~In~~
 491 ~~general~~Generally, all three coupled models enhance the intraseasonal signals over the

492 tropics with discrepancies in detail. ~~By contrast~~Meanwhile, the model mean state does
 493 not substantially improve after coupling. Thus, in this study, the mean state is not the
 494 main contribution to ~~the enhancement of~~enhancing the MJO simulation after coupling.
 495 Instead, coupling leading to rigorous atmosphere–ocean interaction in intraseasonal time
 496 scale is likely the reason for ~~the improvement of~~improving MJO simulation.

498 **3.4 The forecast model: CWBGFS**

499 ~~CWBGFS and CWBGFS SIT were compared for only 3 years. Figure 11~~
 500 ~~demonstrates the wave number frequency spectra and the 10°S–10°N averaged lag–~~
 501 ~~longitude diagrams of CWBGFS between coupled and uncoupled versions. The spectra~~
 502 ~~of CWBGFS SIT suggest better simulation (Fig. 11a, b) in relation to better propagation~~
 503 ~~across the MC (Fig. 11c, d). Although we did not examine the mechanisms in detail, our~~
 504 ~~results demonstrate that MJO forecast skills could be improved by considering the~~
 505 ~~coupling effect in the forecast model.~~

506 **4 Discussion**

507 This study used a one-column TKE-type ocean mixed-layer model SIT coupled
 508 with AGCMs to improve MJO simulation. SIT that is designed to have fine layers near
 509 the surface ~~and can simulate their~~well simulates warm layer, cool skin, and their diurnal
 510 fluctuations. This refined discretization under the ocean surface in SIT provides improved
 511 SST simulation ~~and;~~ thus, improving realistic air–sea interaction. Coupling SIT with
 512 ECHAM5, CAM5, and HiRAM significantly improves the MJO simulation in the three
 513 AGCMs compared with that in the prescribed SST-driven AGCMs. The vertical cross–
 514 section indicates that the strengthened low-level convergence during the preconditioning

格式化: 内文, 行距: 单行间距, 不要贴齐格线

格式化: 不要贴齐格线

515 phase is better simulated in the coupled experiment. Furthermore, the phase variation and
 516 amplitude of the SST and ocean temperature under the surface can be realistically
 517 simulated. Our results reveal that the MJO can be realistically simulated in terms of
 518 strength, period, and propagation speed by increasing the vertical resolution of the one-
 519 column ocean model to better resolve the upper-ocean warm layer.

520 The MSE budget analysis revealed that the coupling effects during the ~~earlier~~
 521 ~~phases~~preconditioning and mature ~~phase~~phases exhibit different contributions. During
 522 the preconditioning phase, the positive contribution of vertical advection and negative
 523 contribution of LH in MSE tendency are closer to realistic values in coupled simulations
 524 during the initial phase of the MJO. ~~During the mature phase of the strongest convection~~
 525 ~~in the MC~~Additionally, the meridional component of the horizontal advection term is the
 526 dominant term during the mature phase of the strongest convection in the MC to enhance
 527 the simulation after coupling. Improved meridional circulation is essential in the coupled
 528 simulations that outperformed uncoupled experiments. The results confirm that the
 529 dominance of dynamic influence over thermodynamic influence in response to the
 530 atmosphere–ocean coupling is the key process ~~leading to the improvement of~~in improving
 531 MJO simulations.

532 In summary, this study suggests two major enhancements of the coupling process.
 533 First, ~~during the preconditioning phase of the MJO over MC~~, the underestimated surface
 534 LH bias in AGCMs can be corrected during the preconditioning phase of the MJO over
 535 MC. Second, during the strongest convection phase over MC, the change in intraseasonal
 536 circulation in the meridional circulation is the dominant factor in coupled simulations
 537 relative to uncoupled experiments. Although many studies have indicated the key role

538 played by the mean state, the mean state in our simulations provides only a secondary
539 contribution to enhancing MJO simulation, with coupling being the main contributor. For
540 example, zonal wind and precipitation changed inconsistently among the three models
541 after coupling. Instead, the meridional gradient of the mean moisture and intraseasonal
542 ~~variance of~~ precipitation have variance has a better relationship after coupling. Therefore,
543 coupling leading to rigorous atmosphere–ocean interaction in the intraseasonal time scale,
544 but ~~not~~ no change in mean states, is likely the reason for MJO simulation improvement.
545 ~~Moreover, coupling SIT with the weather forecast model CWBCFS can improve MJO.~~
546 This study supports previous findings (Tseng et al., 2015) that ~~the enhancement~~
547 ~~of enhancing~~ atmosphere–ocean coupling by considering an extremely high vertical
548 resolution in the first few meters of the ocean model improves MJO simulations, ~~and. It~~
549 also supports that this improvement is independent of AGCMs with different
550 configurations and physical parameterization schemes. Resolving the atmosphere–ocean
551 coupling may be more beneficial than modifying the atmospheric physical
552 parameterization schemes in GCM. In brief, this study suggested the effectiveness of air–
553 sea coupling for improving MJO simulation in a climate model and demonstrated the
554 critical effect of being able to simulate warm layer. Additionally, the findings presented
555 here enhance our understanding of the physical processes that shape the characteristics of
556 the MJO.

557

558 **Code and data availability.** The model code of CAM5-SIT, ECHAM5-SIT and
 559 HiRAM-SIT is available at <https://doi.org/10.5281/zenodo.5701538>,
 560 <https://doi.org/10.5281/zenodo.5510795> and ~~<https://doi.org/10.5281/zenodo.5701579>~~,
 561 ~~<https://doi.org/10.5281/zenodo.5701579>~~. Observational data used in this study include
 562 precipitation from Global Precipitation Climatology Project V1.3 (GPCP, 1° resolution),
 563 ~~outgoing longwave radiation (OLR, OLR~~ (1° resolution), and daily SST (Optimum
 564 Interpolated SST, 0.25° resolution) from the National Oceanic and Atmosphere
 565 Administration, and variables were obtained from the European Centre for Medium-range
 566 Weather Forecast Reanalysis-interim. All experiments were conducted at the National
 567 Center for High-performance Computing. All model codes and data availability presented
 568 here can be obtained by contacting the first author, Dr. Wan-Ling Tseng
 569 (wtseng@gate.sinica.edu.tw).

格式化: 縮排: 第一行: 0 公分, 不要貼齊格線

570
 571 **Author contributions.** HHH and WLT have responsibility for conceptualization,
 572 including analyzing the data and writing the manuscript. YYL, WLL, PHK, BJT, CYT,
 573 and HCL developed the model and provided the simulations.

格式化: 不要貼齊格線

574
 575 **Competing interests.** The authors declare that they have no conflict of interest.

576
 577 **Acknowledgments.** This work was supported by the Taiwan Ministry of Science and
 578 Technology under grant numbers MOST 109-2111-M-001-012-MY3, MOST 110-2811-
 579 M-001-633, and MOST 110-2123-M-001-003. We are grateful to the National Center for
 580 High-Performance Computing for providing computer facilities. The Max Planck
 581 Institute for Meteorology provided ECHAM5.4. We sincerely thank the National Center

格式化: 字型: Times New Roman

582 for Atmospheric Research and their Atmosphere Model Working Group (~~AMWG~~) for
583 release CESM1.2.2. This manuscript was edited by Wallace Academic Editing— and
584 Enago.
585

格式化: 英文(美國)

586 **References**

- 587 ~~Adler, R. F., and Coauthors, 2003: Adler, R. F., Huffman, G. J., Chang, A., Ferraro, R.,~~
 588 ~~Xie, P.-P., Janowiak, J., Rudolf, B., Schneider, U., Curtis, S., and Bolvin, D.:~~ The
 589 version-2 global precipitation climatology project (GPCP) monthly precipitation
 590 analysis (1979-present). ~~J. Journal of Hydrometeorology, 4, 1147-1167, 2003.~~
- 591 Ahn, M. S., ~~Kim, D., Kang, D., Lee, J., Sperber, K. R., Gleckler, P. J., Jiang, X., Ham,~~
 592 ~~Y. G., and Coauthors, 2020: Kim, H.:~~ MJO propagation across the Maritime
 593 Continent: Are CMIP6 models better than CMIP5 models? ~~J. Geophysical~~
 594 ~~Research Letters, 47, e2020GL087250, 2020.~~
- 595 Banzon, V. F., ~~R. W. Reynolds, D. R. W., Stokes, D., and Y. Xue, 2014: Y.:~~ A 1/4-
 596 spatial-resolution daily sea surface temperature climatology based on a blended
 597 satellite and in situ analysis. ~~J. Journal of Climate, 27, 8221-8228, 2014.~~
- 598 Behringer, D., ~~and Y. Xue, 2004: Y.:~~ Evaluation of the global ocean data assimilation
 599 system at NCEP: The Pacific Ocean. ~~J. Proc. Eighth Symp. on Integrated Observing~~
 600 ~~and Assimilation Systems for Atmosphere, Oceans, and Land Surface.~~
- 601 Benedict, J. J., ~~and D. A. Randall, 2011: D. A.:~~ Impacts of Idealized Air–Sea Coupling
 602 on Madden–Julian Oscillation Structure in the Superparameterized CAM. ~~J. Journal~~
 603 ~~of the Atmospheric Sciences, 68, 1990-2008, 10.1175/jas-d-11-04.1, 2011.~~
- 604 Chen, C.-A., ~~H. H. Hsu, C. C. H. H., Hong, P. G. C. C., Chiu, C. Y. P. G., Tu, S. J. C.,~~
 605 ~~Y., Lin, S. J., and A. Kitoh, 2019: A.:~~ Seasonal precipitation change in the western
 606 North Pacific and East Asia under global warming in two high-resolution
 607 AGCMs. ~~J. Climate Dynamics, 53, 5583-5605, 2019.~~
- 608 Chi, N. H., ~~R. C. Lien, E. A. R. C., D'Asaro, E. A., and B. B. Ma, 2014: B. B.:~~ The
 609 surface mixed layer heat budget from mooring observations in the central Indian

格式化: 字型: 12 點

格式化: 字型: 非斜體

格式化: 字型: 非粗體

格式化: 字型: 非斜體

格式化: 字型: 非粗體

格式化: 字型: 非斜體

格式化: 字型: 非粗體

格式化: 字型: 非斜體

格式化: 字型: 非斜體

格式化: 字型: 非粗體

格式化: 字型: 非斜體

格式化: 字型: 非粗體

- 610 Ocean during Madden–Julian Oscillation events. *Journal of Geophysical*
 611 *Research: Oceans*, 119, 4638–4652, 2014. 格式化: 字型: 非斜體
- 612 CLIVAR, M. J. O. W. G., 2009. MJO Simulation Diagnostics. *Journal of Climate*, 22,
 613 3006–3030, 2009. 格式化: 字型: 非粗體
- 614 Dee, D., Uppala, S., Simmons, A., Berrisford, P., Poli, P., Kobayashi, S., Andrae, U.,
 615 ~~Balmaseda, M., Balsamo, G., and Coauthors, 2011:~~Bauer, P.: The ERA-Interim
 616 reanalysis: Configuration and performance of the data assimilation system.
 617 *Quarterly Journal of the Royal Meteorological Society*, 137, 553–597, 2011. 格式化: 字型: 非斜體
格式化: 字型: 非粗體
- 618 Del Genio, A. D., and Y. Chen, 2015: Y.: Cloud-radiative driving of the Madden-Julian
 619 oscillation as seen by the A-Train. *Journal of Geophysical Research:*
 620 *Atmospheres*, 120, 5344–5356, <https://doi.org/10.1002/2015JD023278>, 2015. 格式化: 字型: 非斜體
格式化: 字型: 非粗體
- 621 ~~DeMott, C. A., N. P. DeMott, C. A.,~~ Klingaman, N. P., and S. J. Woolnough, 2015: S. J.:
 622 Atmosphere-ocean coupled processes in the Madden-Julian oscillation. *Reviews*
 623 *of Geophysics*, 53, 1099–1154, 2015. 格式化: 字型: 非斜體
格式化: 字型: 非粗體
- 624 ~~DeMott, C. A., DeMott, C. A., J. J. Benedict, N. P. J. J.,~~ Klingaman, S. J. N. P.,
 625 Woolnough, S. J., and D. A. Randall, 2016: D. A.: Diagnosing ocean feedbacks to
 626 the MJO: SST-modulated surface fluxes and the moist static energy budget.
 627 *Journal of Geophysical Research: Atmospheres*, 121, 8350–8373, 2016. 格式化: 字型: 非斜體
格式化: 字型: 非粗體
- 628 DeMott, C. A., N. P. Klingaman, W. L. N. P., Tseng, M. A. W. L., Burt, Y. M. A., Gao,
 629 Y., and D. A. Randall, 2019: D. A.: The convection connection: How ocean
 630 feedbacks affect tropical mean moisture and MJO propagation. *Journal of*
 631 *Geophysical Research: Atmospheres*, 124, 11910–11931, 2019. 格式化: 字型: 非斜體
格式化: 字型: 非粗體

- 632 Drushka, K., ~~J.~~Sprintall, ~~S.~~T.J., Gille, ~~S.~~T., and ~~S.~~Wijffels, ~~2012~~:~~S.~~: In situ
633 observations of Madden-Julian Oscillation mixed layer dynamics in the Indian and
634 western Pacific Oceans. ~~J.~~Journal of Climate, ~~25~~, 2306-2328, ~~2012~~.
- 635 Duchon, C. E., ~~1979~~:. Lanczos filtering in one and two dimensions. ~~J.~~Journal of Applied
636 Meteorology and Climatology, ~~18~~, 1016-1022, ~~1979~~.
- 637 Flatau, M., ~~P.~~J.Flatau, P. ~~J.~~, Phoebus, ~~P.~~, and ~~P.~~P.Niiler, ~~1997~~:~~P.~~ P.: The feedback
638 between equatorial convection and local radiative and evaporative processes: The
639 implications for intraseasonal oscillations. ~~J.~~Journal of the atmospheric sciences, ~~54~~,
640 2373-2386, ~~1997~~.
- 641 Fu, X., ~~Wang, W., Lee, J.-Y., Wang, B., Kikuchi, K., Xu, J., Li, J., and Coauthors,~~
642 ~~2015~~:~~Weaver, S.~~: Distinctive roles of air–sea coupling on different MJO events: A
643 new perspective revealed from the DYNAMO/CINDY field campaign. ~~J.~~Monthly
644 Weather Review, ~~143~~, 794-812, ~~2015~~.
- 645 Gaspar, P., ~~Y.~~Gregoris, ~~Y.~~, and ~~J.~~M.Lefevre, ~~1990~~:~~J.~~M.: A simple eddy kinetic
646 energy model for simulations of the oceanic vertical mixing: Tests at station Papa
647 and long-term upper ocean study site. ~~J.~~Journal of Geophysical Research: Oceans,
648 ~~95~~, 16179-16193, ~~1990~~.
- 649 Hendon, H. H., ~~and M.~~L.Salby, ~~1994~~:~~M.~~ L.: The life cycle of the Madden-Julian
650 oscillation. ~~J.~~Journal of the Atmospheric Sciences, ~~51~~, 2225-2237, ~~1994~~.
- 651 Hendon, H. H., ~~B.~~Liebmann, ~~B.~~, and ~~J.~~D.Glick, ~~1998~~:~~J.~~ D.: Oceanic Kelvin waves and
652 the Madden – Julian oscillation. ~~J.~~Journal of the Atmospheric Sciences, ~~55~~, 88-101,
653 ~~1998~~.
- 654 ~~Hong, S. Y., and H. L. Pan, 1996: Nonlocal boundary layer vertical diffusion in a~~
655 ~~medium-range forecast model. Monthly weather review, 124, 2322–2339.~~

格式化: 字型: 非斜體

格式化: 字型: 非粗體

格式化: 字型: 非斜體

格式化: 字型: 非粗體

格式化: 字型: 非斜體

格式化: 字型: 非粗體

格式化: 字型: 非斜體

格式化: 字型: 非粗體

格式化: 字型: 非斜體

格式化: 字型: 非粗體

格式化: 字型: 非斜體

格式化: 字型: 非粗體

格式化: 字型: 非斜體

格式化: 字型: 非粗體

- 656 Hsu, P.-C., and ~~T.~~Li, ~~2012~~:T.: Role of the Boundary Layer Moisture Asymmetry in
 657 Causing the Eastward Propagation of the Madden-Julian Oscillation~~**~~, Journal of
 658 Climate, 25, 4914-4931, 2012.
- 659 Hurrell, J. W., ~~Holland, M. M., Gent, P. R., Ghan, S., Kay, J. E., Kushner, P. J.,~~
 660 ~~Lamarque, J.-F., Large, W. G., Lawrence, D., and Coauthors, 2013~~:Lindsay, K.:
 661 The community earth system model: a framework for collaborative research,
 662 Bulletin of the American Meteorological Society, 94, 1339-1360, 2013.
- 663 Inness, P. M., ~~J.-M.~~Slingo, ~~E.-J. M.~~, Guilyardi, ~~E.~~, and ~~J.-~~Cole, ~~2003~~:J.: Simulation of
 664 the Madden-Julian Oscillation in a coupled general circulation model. Part II: The
 665 role of the basic state,
 666 Journal of Climate, 16, 365-382, 2003.
- 666 Jiang, X., ~~Á. F.~~Adames, ~~M. Á. F.~~, Zhao, ~~D.-M.~~, Waliser, ~~D.~~, and ~~E.-~~Maloney, ~~2018~~:E.: A
 667 unified moisture mode framework for seasonality of the Madden-Julian
 668 oscillation,
 669 Journal of Climate, 31, 4215-4224, 2018.
- 669 ~~Jiang, X., and Coauthors, 2020~~:Jiang, X., Adames, Á. F., Kim, D., Maloney, E. D., Lin,
 670 ~~H., Kim, H., Zhang, C., DeMott, C. A., and Klingaman, N. P.~~: Fifty years of
 671 research on the Madden-Julian Oscillation: Recent progress, challenges, and
 672 perspectives,
 673 Journal of Geophysical Research: Atmospheres, 125,
 674 e2019JD030911, 2020.
- 674 Kang, I.-S., ~~F.~~Liu, ~~M.-S.F.~~, Ahn, ~~Y.-M.-S.~~, Yang, ~~Y.-M.~~, and ~~B.-~~Wang, ~~2013~~:B.: The
 675 Role of SST Structure in Convectively Coupled Kelvin-Rossby Waves and Its
 676 Implications for MJO Formation,
 677 Journal of Climate, 26, 5915-5930, 2013.
- 677 Kim, D., ~~A.-H.~~Sobel, ~~E.-D.A. H.~~, Maloney, ~~E. D.-M.~~, Frierson, ~~D. M.~~, and ~~I.-S.~~Kang,
 678 ~~2011~~:I.-S.: A systematic relationship between intraseasonal variability and mean
 679 state bias in AGCM simulations,
 679 Journal of Climate, 24, 5506-5520, 2011.

格式化: 字型: 非斜體

格式化: 字型: 非粗體

格式化: 字型: 非斜體

格式化: 字型: 非粗體

格式化: 字型: 非斜體

格式化: 字型: 非粗體

格式化: 字型: 非斜體

格式化: 字型: 非粗體

格式化: 字型: 非斜體

格式化: 字型: 非粗體

格式化: 字型: 非斜體

格式化: 字型: 非粗體

格式化: 字型: 非斜體

格式化: 字型: 非粗體

- 680 Kim, D., ~~Sperber, K., Stern, W., Waliser, D., Kang, I.-S., Maloney, E., Wang, W.,~~
 681 ~~Weickmann, K., Benedict, J., and Coauthors, 2009:~~Khairoutdinov, M.: Application
 682 of MJO simulation diagnostics to climate models. *Journal of climate*, 22, 6413-
 683 6436, 2009.
- 684 Kim, H.-M., ~~P.-J. Webster, V.-E. P. J., Toma, V. E., and D.-Kim, 2014:~~D.: Predictability
 685 and prediction skill of the MJO in two operational forecasting systems. *Journal of*
 686 *Climate*, 27, 5364-5378, 2014.
- 687 Klingaman, N., and S.-Woolnough, 2013:S.: The role of air–sea coupling in the
 688 simulation of the Madden–Julian oscillation in the Hadley Centre model.
 689 *Quarterly Journal of the Royal Meteorological Society*, 2013.
- 690 Klingaman, N. P., and C.-A.-Demott, 2020:C. A.: Mean state biases and interannual
 691 variability affect perceived sensitivities of the Madden-Julian Oscillation to air-sea
 692 coupling. *Journal of Advances in Modeling Earth Systems*, 12, e2019MS001799.
 693 2020.
- 694 Krishnamurti, T. N., ~~D.-Oosterhof, D., and A.-Mehta, 1988:~~A.: Air–sea interaction on
 695 the time scale of 30 to 50 days. *Journal of the atmospheric sciences*, 45, 1304-
 696 1322, 1988.
- 697 ~~Li, C. W., and J. Wang, 2000: Large eddy simulation of free surface shallow water~~
 698 ~~flow. *International journal for numerical methods in fluids*, 34, 31–46.~~
- 699 ~~Li, Y., and R. E.-Lan, Y.-Y., Tsuang, B.-J., Tu, C.-Y., Wu, T.-Y., Chen, Y.-L., and~~
 700 ~~Hsieh, C.-I.: Observation and simulation of meteorology and surface energy~~
 701 ~~components over the South China Sea in summers of 2004 and 2006, *Terrestrial,*~~
 702 ~~*Atmospheric and Oceanic Sciences*, 21, 325-342, 2010.~~

格式化: 字型: 非斜體

格式化: 字型: 非粗體

格式化: 字型: 非斜體

格式化: 字型: 非粗體

格式化: 字型: 非斜體

格式化: 字型: 非斜體

格式化: 字型: 非粗體

格式化: 字型: 非斜體

格式化: 字型: 非粗體

- 703 [Lan, Y. Y., Hsu, H. H., Tseng, W. L., and Jiang, L. C.: Embedding a One-column](#)
 704 [Ocean Model \(SIT 1.06\) in the Community Atmosphere Model 5.3 \(CAM5.3;](#)
 705 [CAM5-SIT v1.0\) to Improve Madden-Julian Oscillation Simulation in Boreal](#)
 706 [Winter, Geosci. Model Dev. Discuss., 2021, 1-49, 10.5194/gmd-2021-346, 2021.](#)
- 707 [Li, Y. and Carbone, 2012; R. E.: Excitation of Rainfall over the Tropical Western](#)
 708 [Pacific, Journal of the Atmospheric Sciences, 69, 2983-2994, 10.1175/jas-d-11-](#)
 709 [0245.1, 2012.](#)
- 710 [Liebmann, B., 1996: Description of a complete \(interpolated\) outgoing longwave](#)
 711 [radiation dataset, Bull. Amer. Meteor. Soc., 77, 1275-1277, 1996.](#)
- 712 [Liou, C. S., and Coauthors, 1997: The second generation global forecast system at the](#)
 713 [central weather bureau in Taiwan, Weather and Forecasting, 12, 653-663.](#)
- 714 [Madden, R. A., and Julian, P. R.: Julian, 1972: Description of global-scale circulation](#)
 715 [cells in the tropics with a 40-50 day period, J. Atmos. Sci., 29, 1109-1123, 1972.](#)
- 716 [Marshall, A. G., Alves, O., and Hendon, 2008; H. H.: An Enhanced Moisture](#)
 717 [Convergence-Evaporation Feedback Mechanism for MJO Air-Sea Interaction,](#)
 718 [Journal of the Atmospheric Sciences, 65, 970-986, 10.1175/2007jas2313.1, 2008.](#)
- 719 [Matthews, A. J., Singhruck, P., and Heywood, 2007; K. J.: Deep ocean impact of](#)
 720 [a Madden-Julian Oscillation observed by Argo floats, Science, 318, 1765-1769,](#)
 721 [2007.](#)
- 722 [Matthews, A. J., Baranowski, D. B., Heywood, K. J., Flatau, P. J., and Schmidtko, S.:](#)
 723 [The surface diurnal warm layer in the Indian Ocean during CINDY/DYNAMO,](#)
 724 [Journal of Climate, 27, 9101-9122, 2014.](#)
- 725 [McPhaden, M. J., Busalacchi, A. J., and Anderson, 2010; D. L.: A toga](#)
 726 [retrospective, Oceanography, 23, 86-103, 2010.](#)

格式化: 字型: 非斜體

格式化: 字型: 非粗體

格式化: 字型: 非斜體

格式化: 字型: 非粗體

格式化: 字型: 非斜體

格式化: 字型: 非粗體

格式化: 字型: 非斜體

格式化: 字型: 非粗體

格式化: 字型: 非斜體

格式化: 字型: 非粗體

格式化: 字型: 非斜體

格式化: 字型: 非粗體

- 727 Mellor, G. L. and Yamada, T.: Development of a turbulence closure model for
 728 geophysical fluid problems, Reviews of Geophysics, 20, 851-875, 1982.
- 729 Nordeng, T. E., ~~1994:~~ Extended versions of the convective parametrization scheme at
 730 ECMWF and their impact on the mean and transient activity of the model in the
 731 tropics, European Centre for Medium-Range Weather ~~Forecasts~~Forecasts1994.
- 732 Oliver, E., and ~~K.~~Thompson, ~~2011:~~K.: Sea level and circulation variability of the Gulf
 733 of Carpentaria: Influence of the Madden-Julian Oscillation and the adjacent deep
 734 ocean, Journal of Geophysical Research: Oceans, 116, 2011.
- 735 Park, S. and Bretherton, C. S.: The University of Washington shallow convection and
 736 moist turbulence schemes and their impact on climate simulations with the
 737 Community Atmosphere Model, Journal of Climate, 22, 3449-3469, 2009.
- 738 Roeckner, E., ~~2003:~~ The atmospheric general circulation model ECHAM5: Part 1:
 739 model description, Max-Planck-Institut fuer ~~Meteorologie~~Meteorologie2003.
- 740 ~~Roeckner, E., and Coauthors, 2006:~~Roeckner, E., Brokopf, R., Esch, M., Giorgetta, M.,
 741 ~~Hagemann, S., Kornblueh, L., Manzini, E., Schlese, U., and Schulzweida, U.:~~
 742 Sensitivity of simulated climate to horizontal and vertical resolution in the
 743 ECHAM5 atmosphere model, Journal of Climate, 19, 3771-3791, 2006.
- 744 Salby, M. L., and ~~H. H.~~Hendon, ~~1994:~~H. H.: Intraseasonal behavior of clouds,
 745 temperature, and motion in the tropics, Journal of the Atmospheric Sciences, 51,
 746 2207-2224, 1994.
- 747 Shinoda, T., and ~~H. H.~~Hendon, ~~1998:~~H. H.: Mixed layer modeling of intraseasonal
 748 variability in the tropical western Pacific and Indian Oceans, Journal of Climate,
 749 11, 2668-2685, 1998.

格式化: 字型: 非斜體

格式化: 字型: 非斜體

格式化: 字型: 非粗體

格式化: 字型: 非斜體

格式化: 字型: 非斜體

格式化: 字型: 非粗體

格式化: 字型: 非斜體

格式化: 字型: 非粗體

格式化: 字型: 非斜體

格式化: 字型: 非粗體

- 750 ~~Shinoda, T., H. H. Hendon, and J. Glick, 1998: Intraseasonal variability of surface~~
 751 ~~fluxes and sea surface temperature in the tropical western Pacific and Indian~~
 752 ~~Oceans. *Journal of climate*, **11**, 1685-1702.~~
- 753 Sobel, A. H., ~~E. D.~~ Maloney, ~~G. E. D.~~ Bellon, ~~G.~~, and ~~D. M.~~ Frierson, ~~2008: D. M.~~: The
 754 role of surface heat fluxes in tropical intraseasonal oscillations. *Nature*
 755 *Geoscience*, **1**, 653-657, 2008.
- 756 ~~---~~, 2010: Sobel, A. H., Maloney, E. D., Bellon, G., and Frierson, D. M.: Surface
 757 fluxes and tropical intraseasonal variability: A reassessment. *Journal of Advances*
 758 *in Modeling Earth Systems*, **2**, 2010.
- 759 Team, G. G. A. M. D., ~~and Coauthors,~~ 2004: Anderson, J. L., Balaji, V., Broccoli, A. J.,
 760 Cooke, W. F., Delworth, T. L., Dixon, K. W., Donner, L. J., Dunne, K. A., and
 761 Freidenreich, S. M.: The new GFDL global atmosphere and land model AM2–
 762 LM2: Evaluation with prescribed SST simulations. *Journal of Climate*, **17**, 4641–
 763 4673, 2004.
- 764 Tseng, W.-L., ~~B. J.~~ Tsuang, ~~N. B. J.~~, Keenlyside, ~~H. H. N.~~, Hsu, ~~H. H.~~, and ~~C. Y.~~ Tu,
 765 ~~2015: C. Y.~~ Resolving the upper-ocean warm layer improves the simulation of the
 766 Madden–Julian oscillation. *Climate Dynamics*, **1-17**, 10.1007/s00382-014-2315-1,
 767 2015.
- 768 Tsuang, B.-J., ~~C. Y. Tu, J. L. Tu, C.-Y., and Arpe, K.~~: Lake parameterization for
 769 climate models. Max-Planck-Institute for Meteorology Rept, 316, 72pp, 2001.
- 770 Tsuang, B.-J., Tu, C.-Y., Tsai, J.-A.-L., Dracup, K. J. A., Arpe, K., and T. Meyers,
 771 2009: T. A more accurate scheme for calculating Earth's-skin temperature. *Climate*
 772 *Dynamics*, **32**, 251-272, 2009.

格式化: 字型: 非斜體

格式化: 字型: 非粗體

格式化: 字型: 非斜體

格式化: 字型: 非粗體

格式化: 字型: 非斜體

格式化: 字型: 非粗體

格式化: 字型: 非斜體

格式化: 字型: 非粗體

格式化: 字型: 非斜體

格式化: 字型: 非粗體

- 773 Tu, C.-Y.: Sea Surface Temperature Simulation in Climate Model, Department of
 774 Environmental Engineering, National Chung Hsing University, 2006.
- 775 Tu, C.-Y. and B.-J. Tsuang, 2005:B.-J.: Cool-skin simulation by a one-column ocean
 776 model., Geophysical research letters, 32, 2005.
- 777 Tu, C.-Y. and Tsuang, B.-J.: Numerical discretization for sea surface temperature
 778 simulation in a turbulent kinetic energy ocean model, 2014.
- 779 Wang, B. and H.-Rui, 1990:H.: Dynamics of the Coupled Moist Kelvin-Rossby Wave
 780 on an Equatorial-Plane., Journal of the Atmospheric Sciences, 47, 397-413, 1990.
- 781 Wang, B. and X.-Xie, 1998:X.: Coupled modes of the warm pool climate system. Part
 782 I: The role of air-sea interaction in maintaining Madden-Julian oscillation.,
 783 Journal of Climate, 11, 2116-2135, 1998.
- 784 Wang, G., Z.-Ling, R.-Z., Wu, R., and C.-Chen, 2013:C.: Impacts of the Madden-Julian
 785 oscillation on the summer South China Sea ocean circulation and temperature.,
 786 Journal of climate, 26, 8084-8096, 2013.
- 787 Wang, Y. C., W. L. Tseng, and H. H. Hsu, 2021: Role of Convection-circulation
 788 Coupling in the Propagation Mechanism of the Madden-Julian Oscillation over the
 789 Maritime Continent in Climate Models.
- 790 Watterson, I. and J.-Syktus, 2007:I.: The influence of air-sea interaction on the
 791 Madden-Julian oscillation: The role of the seasonal mean state., Climate dynamics,
 792 28, 703-722, 2007.
- 793 Webber, B. G., A.-J. Matthews, A. J., and K.-J. Heywood, 2010:K. J.: A dynamical
 794 ocean feedback mechanism for the Madden-Julian oscillation., Quarterly Journal
 795 of the Royal Meteorological Society: A journal of the atmospheric sciences,
 796 applied meteorology and physical oceanography, 136, 740-754, 2010.

格式化: 字型: 非斜體

格式化: 字型: 非粗體

格式化: 字型: 非斜體

格式化: 字型: 非粗體

格式化: 字型: 非斜體

格式化: 字型: 非粗體

格式化: 字型: 非斜體

格式化: 字型: 非粗體

格式化: 字型: 非斜體

格式化: 字型: 非粗體

格式化: 字型: 非斜體

格式化: 字型: 非粗體

- 797 Webber, B. G., ~~A. J. Matthews~~, ~~K. A. J.~~, Heywood, ~~K. J.~~, and ~~D. P. Stevens~~, ~~2012~~:~~D. P.~~:
 798 Ocean Rossby waves as a triggering mechanism for primary Madden-Julian
 799 events. ~~Quarterly Journal of the Royal Meteorological Society~~, ~~138~~, 514-527.
 800 ~~2012~~.
- 801 Wheeler, M. C., ~~and H. H. Hendon~~, ~~2004~~:~~H. H.~~: An all-season real-time multivariate
 802 MJO index: Development of an index for monitoring and prediction. ~~Monthly~~
 803 ~~Weather Review~~, ~~132~~, 1917-1932, ~~2004~~.
- 804 Woolnough, S. J., ~~J. M. Slingo~~, ~~J. M.~~, and ~~B. J. Hoskins~~, ~~2000~~:~~B. J.~~: The relationship
 805 between convection and sea surface temperature on intraseasonal timescales.
 806 ~~Journal of Climate~~, ~~13~~, 2086-2104, ~~2000~~.
- 807 ~~Yanai, M., S. Esbensen, and J. H. Chu, 1973: Determination of bulk properties of~~
 808 ~~tropical cloud clusters from large scale heat and moisture budgets. *Journal of the*~~
 809 ~~*Atmospheric Sciences*, ~~30~~, 611-627.~~
- 810 Zhang, C., ~~2005~~:. Madden-Julian oscillation. ~~Reviews of Geophysics~~, ~~43~~, ~~2005~~.
 811 ~~Zhang, G. J. and McFarlane, N. A.: Sensitivity of climate simulations to the~~
 812 ~~parameterization of cumulus convection in the Canadian Climate Centre general~~
 813 ~~circulation model. *Atmosphere-ocean*, ~~33~~, 407-446, 1995.~~
- 814 Zhao, M., ~~I. M. Held~~, ~~S. J. I. M.~~, Lin, ~~S. J.~~, and ~~G. A. Vecchi~~, ~~2009~~:~~G. A.~~: Simulations
 815 of global hurricane climatology, interannual variability, and response to global
 816 warming using a 50-km resolution GCM. ~~Journal of Climate~~, ~~22~~, 6653-6678.
 817 ~~2009~~.
- 818

格式化: 字型: 非斜體

格式化: 字型: 非粗體

格式化: 字型: 非斜體

格式化: 字型: 非粗體

格式化: 字型: 非斜體

格式化: 字型: 非粗體

格式化: 字型: 非斜體

格式化: 字型: 非粗體

格式化: 字型: 非斜體

格式化: 字型: 非粗體

← 格式化: 不要貼齊格線

	ECHAM5-SIT	CAM5-SIT	HiRAM-SIT	CWBGFS-SIT
AGCM	ECHAM5	CAM5	HiRAM	CWBGFS
Horizontal resolution	T63(~2°)	1.9°x2°x2.5°	1°x1°x1°	T319
SST	OISST	OISST	OISST	OISST
BC SIC	OISST	OISST	OISST	OISST
OT/OS	GODAS	GODAS	GODAS	GODAS
Atmosphere vertical resolution	L31	L30	L32	L60
Ocean vertical resolution	42	42	42	42
Coupled region	30°S-30°N	30°S-30°N	30°S-30°N 30°N blending interpolated	30°S-30°N, 30°-40°
Time	1985-2005 (21 years)		2012-2014 (3 years)	

- 刪除儲存格
- 格式化: 字型: 12 點
- 格式化: 行距: 2 倍行高, 不要貼齊格線
- 格式化表格
- 格式化: 字型: 12 點
- 格式化: 行距: 2 倍行高, 不要貼齊格線
- 格式化: 字型: 12 點
- 格式化: 行距: 2 倍行高, 不要貼齊格線
- 格式化: 字型: 12 點
- 格式化: 字型: 12 點
- 格式化: 行距: 2 倍行高, 不要貼齊格線
- 格式化: 行距: 2 倍行高, 不要貼齊格線
- 格式化: 字型: 12 點
- 格式化: 行距: 2 倍行高, 不要貼齊格線
- 格式化: 字型: 12 點
- 格式化: 行距: 2 倍行高, 不要貼齊格線
- 格式化: 字型: 12 點
- 格式化: 行距: 2 倍行高, 不要貼齊格線
- 刪除儲存格
- 格式化: 行距: 2 倍行高, 不要貼齊格線
- 格式化: 不要貼齊格線

819
820
821

Table 1. Detailed information of models and experiments.

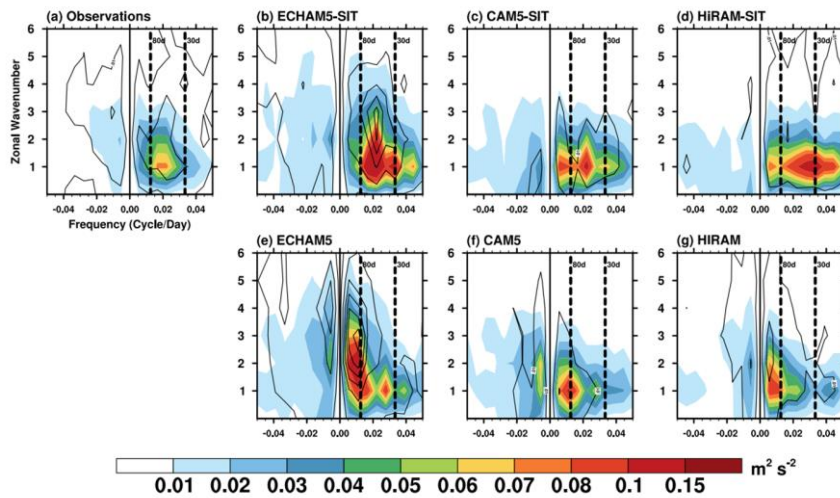
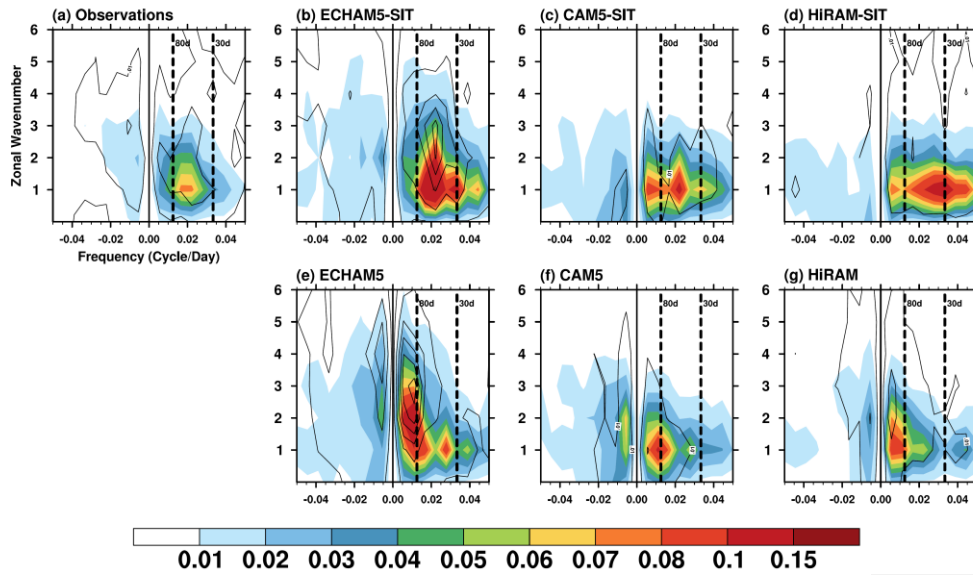


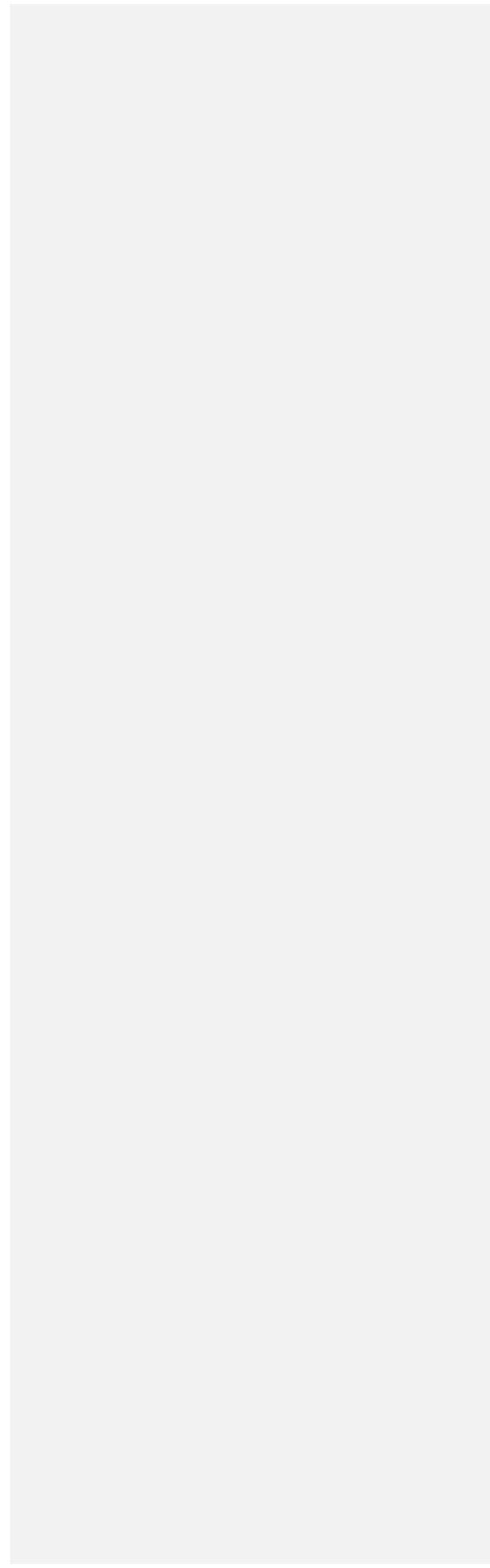
Figure 1. Wave number–frequency spectra for equatorial 850-hPa zonal wind (shading; $\text{m}^2 \text{s}^{-2}$) and precipitation (contours; $\text{mm}^2 \text{day}^{-2}$) over 10°S – 10°N from (a) observations and simulations by using the (b–d) coupled and (e–g) uncoupled AGCM.

格式化: 不要貼齊格線

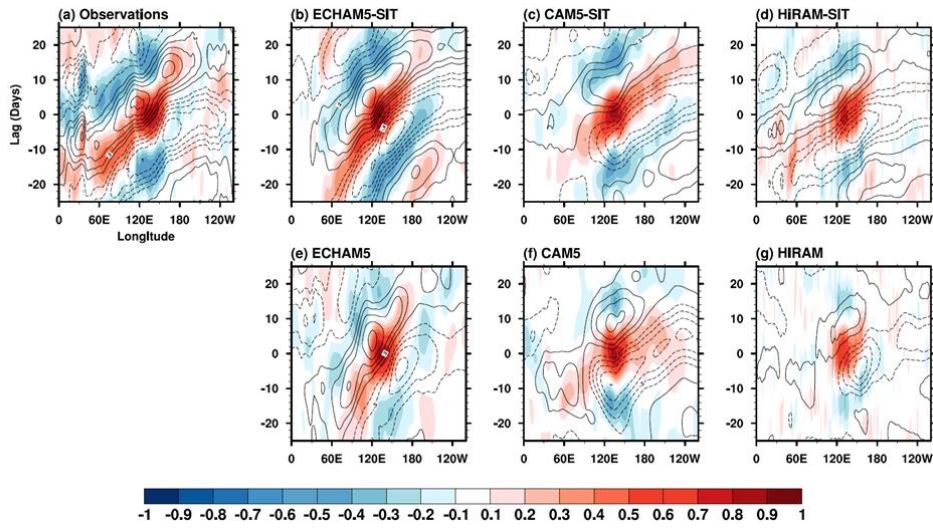
828

41

41



829



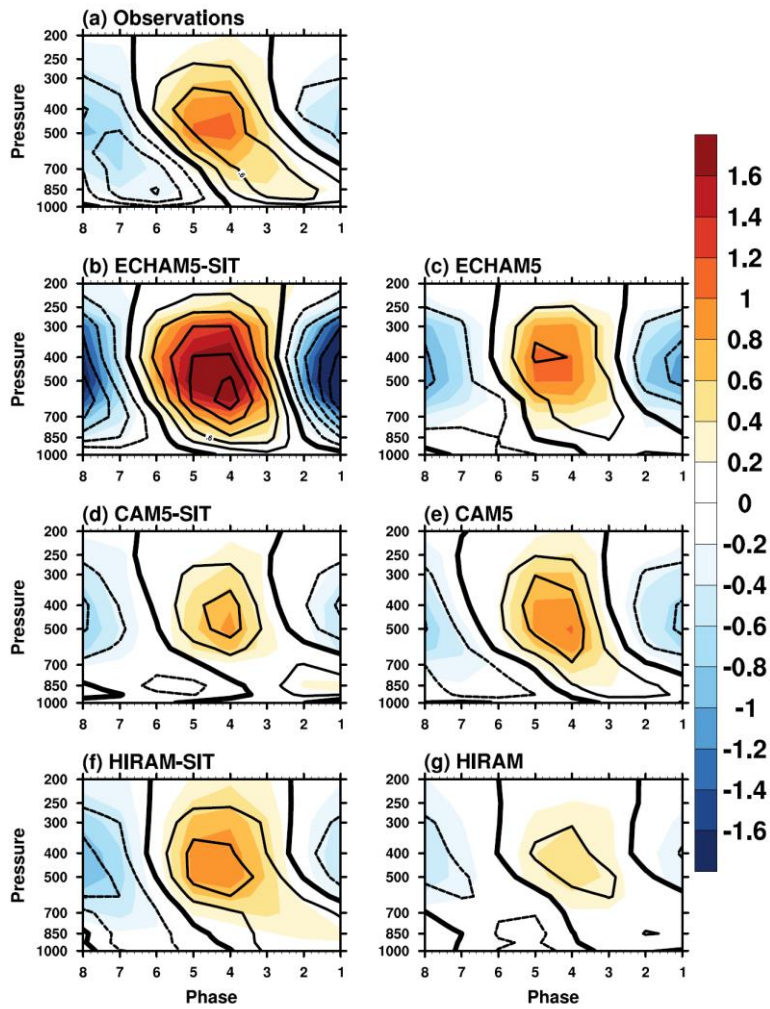
830

831 **Figure 2.** The 10°S – 10°N averaged lag–longitude diagrams of intraseasonal precipitation
 832 (shading) and 10-m zonal wind (contour) correlated against precipitation at region (10°S –
 833 5°N , 120°E – 150°E) from (a) observations and simulations ~~by~~ using the (b–d) coupled
 834 and (e–g) uncoupled AGCM. The contour interval is 0.1.

格式化: 字型: 粗體

835

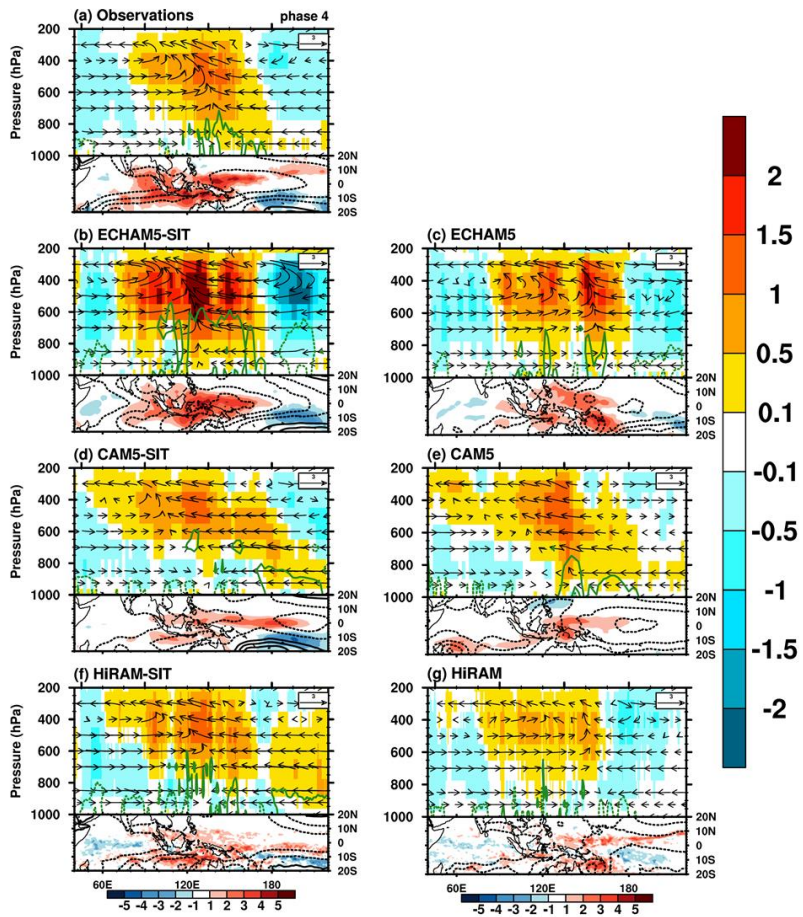
836



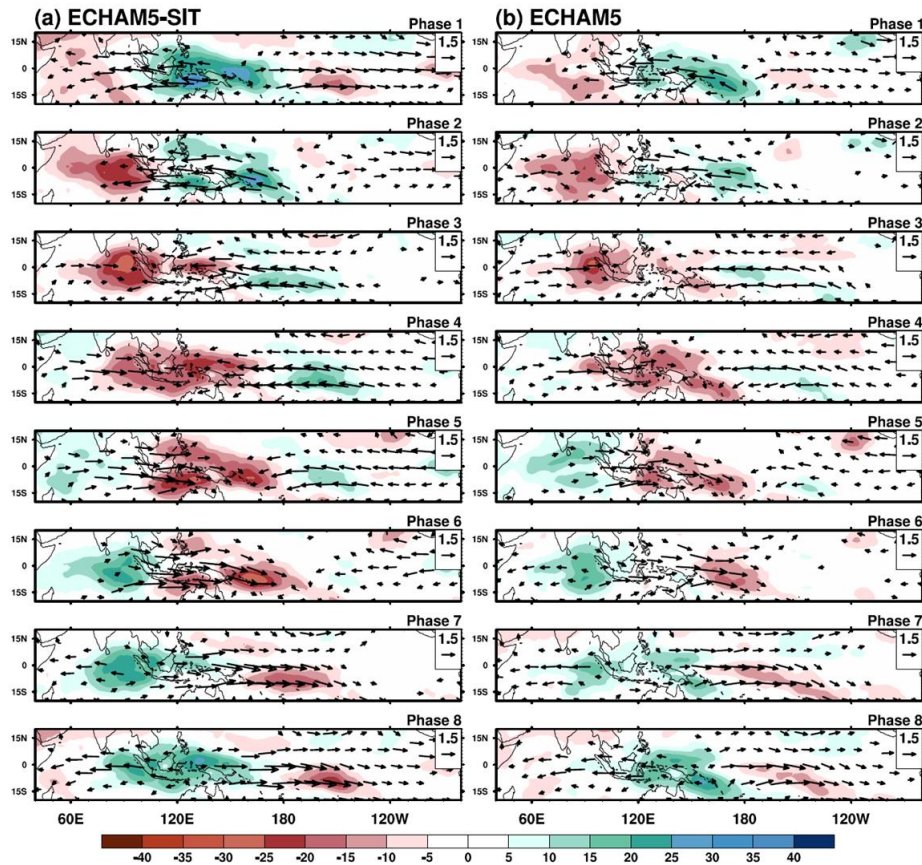
837

838 **Figure 3.** Vertical profiles with respect to MJO phases averaged over 10°S–EQ and
 839 120°E–150°E for intraseasonal anomalies (i.e., with 20–100 day filtering) of Q1 (shading;
 840 K day^{-1}) and Q2 (contours; K day^{-1}) from (a) observations and simulations by using the
 841 (b–d) coupled and (e–g) uncoupled AGCM.

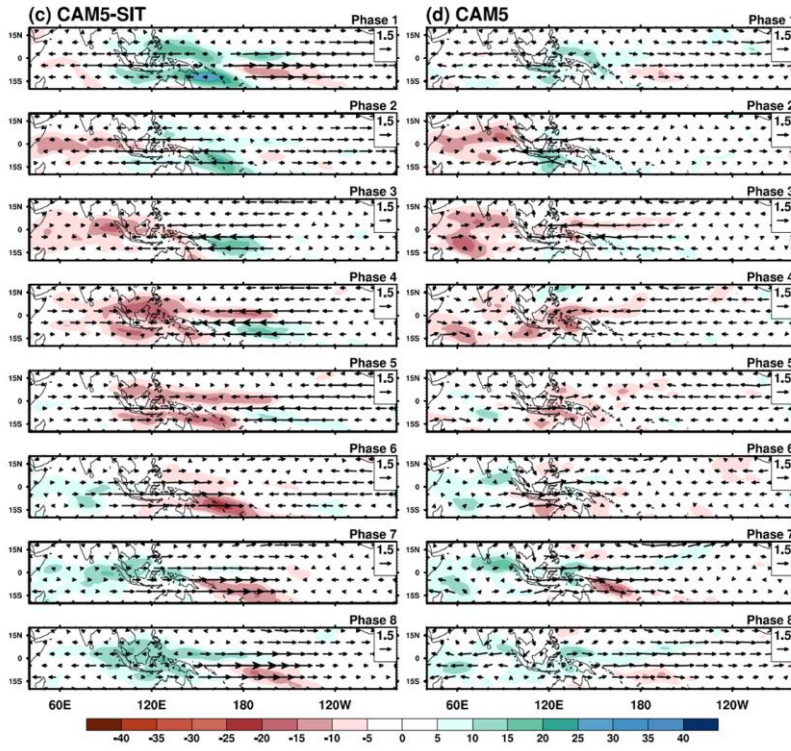
842



843



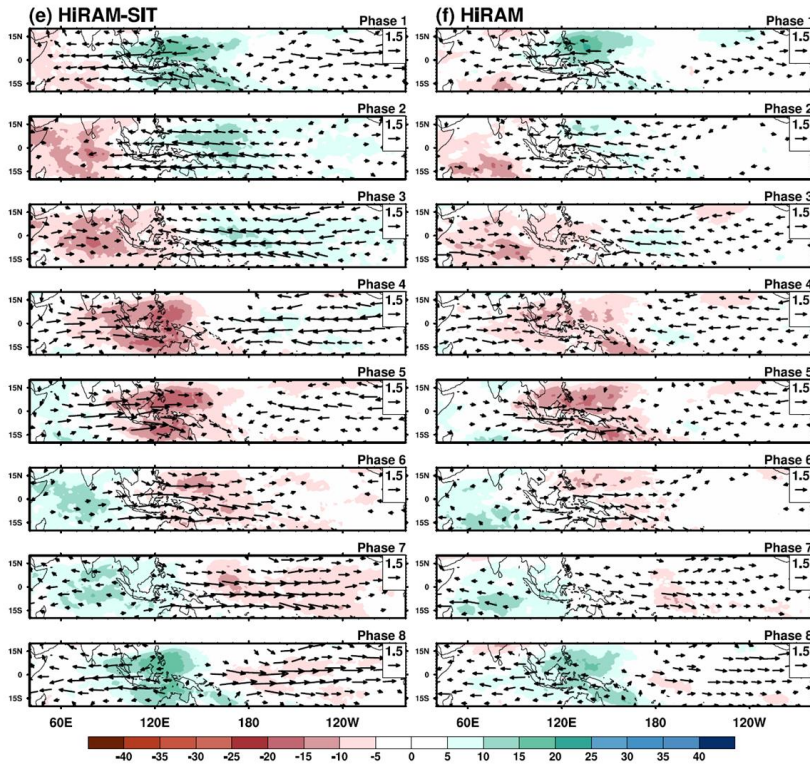
844 **Figure 3.** Composite November–April 20–100-day OLR ($W m^{-1}$; color) and 10-m surface
 845 wind anomalies ($m s^{-1}$; vectors) as a function of the MJO phase in (a) ECHAM5-SIT and
 846 (b) ECHAM5. Vectors $<0.6 m s^{-1}$ are not shown. The reference vector in units of $m s^{-1}$ is
 847 shown at the bottom right. The number of days used to generate the composite for each
 848 phase is shown to the right of each panel.
 849
 850



851

852 **Figure 3.** continued, (c) CAM5-SIT and (d) CAM5.

853

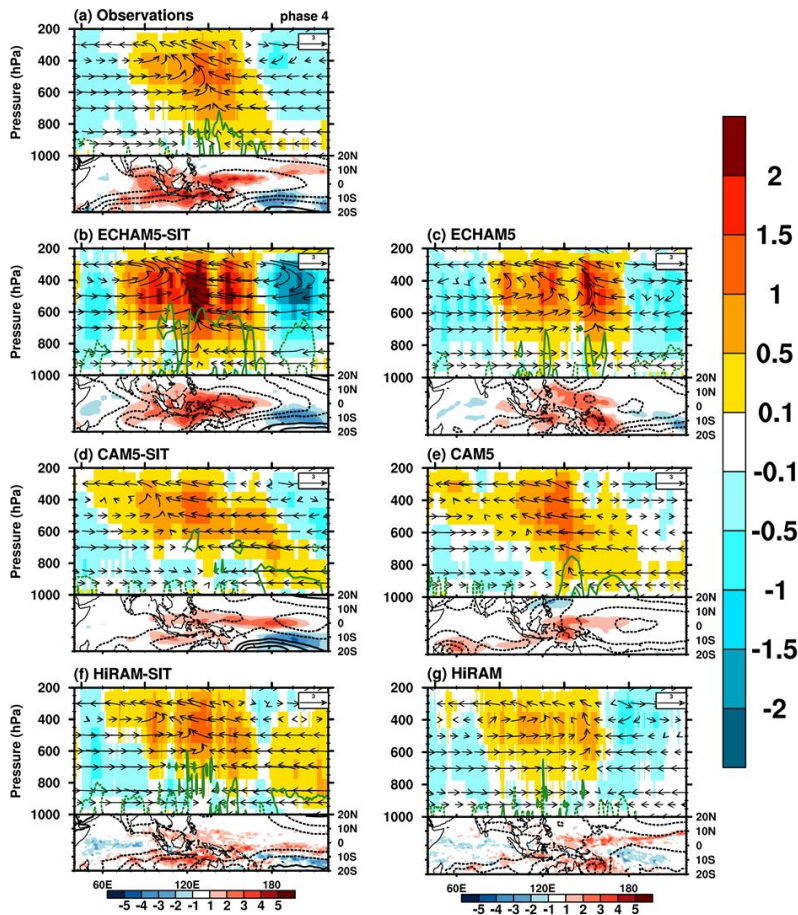


854

855 **Figure 3. continued, (e) HiRAM-SIT and (f) HiRAM.**

856

857



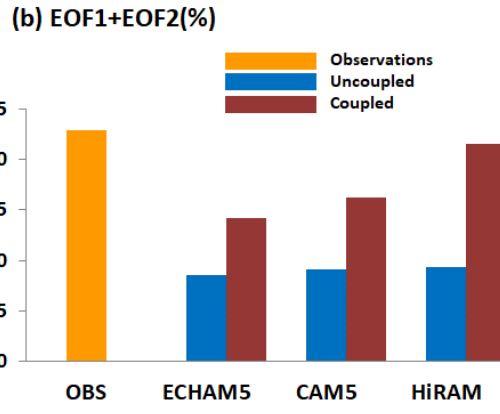
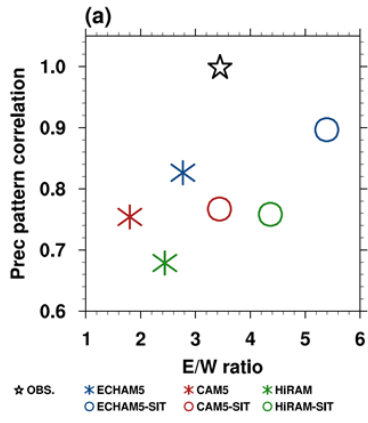
858

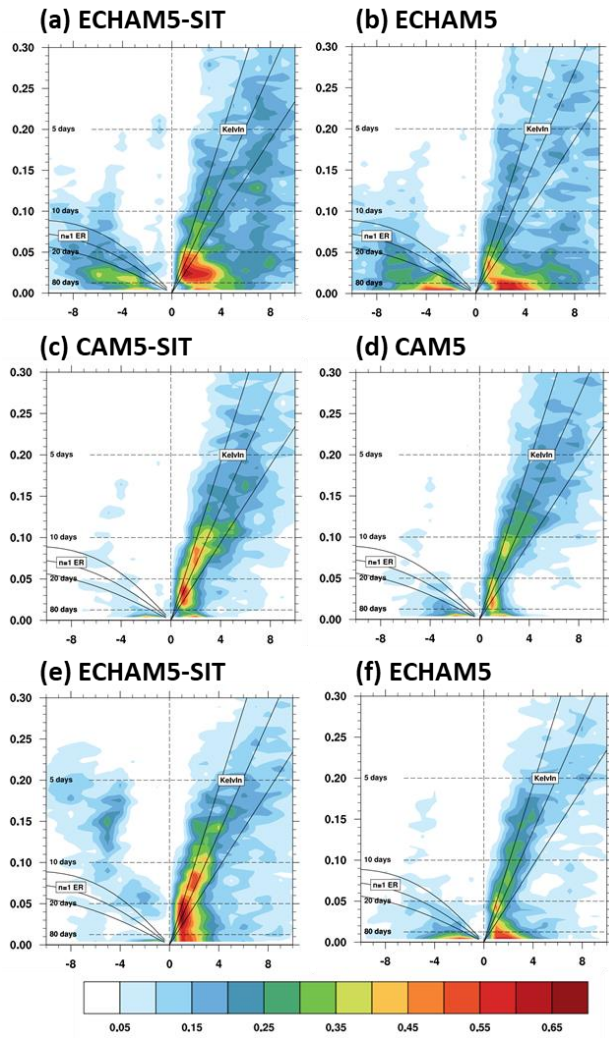
859 **Figure 4.** Structure of simulated MJO in phase 4. The longitude–height cross-sections
 860 (averaged over 10°S–EQ) of the MJO scaled wind circulation (vector, u : m s^{-1} , ω :
 861 $10^{-2} \text{ Pa s}^{-1}$), $Q1$ (shading, unit: K day^{-1}), and the horizontal moisture convergence
 862 (green contour, unit: $10^{-6} \text{ g kg}^{-1} \text{ s}^{-1}$) from (a) observations and simulations **by**-using the
 863 (b–d) coupled and (e–g) uncoupled **AGCMAGCMs**. The contour interval of the moisture
 864 convergence is $8 \times 10^{-6} \text{ g kg}^{-1} \text{ s}^{-1}$; solid line is positive. Precipitation (shading, unit:

格式化: 不要貼齊格線

865 mm day⁻¹) and sea level pressure (contour, unit: hPa). Contour interval of sea level
866 pressure is 30 hPa; dashed line indicates negative.

867





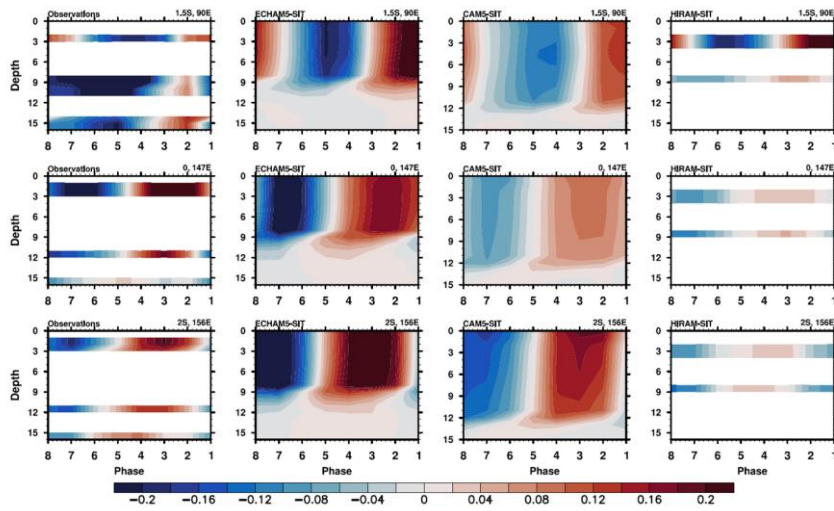
869

870 **Figure 5.** Symmetric wavenumber–frequency spectra of 10°N–10°S-averaged

871 850-hPa zonal wind using the (a, c, e) coupled and (b, d, f) uncoupled AGCMs. Units:

872 $\text{m}^2 \text{s}^{-2}$.

873



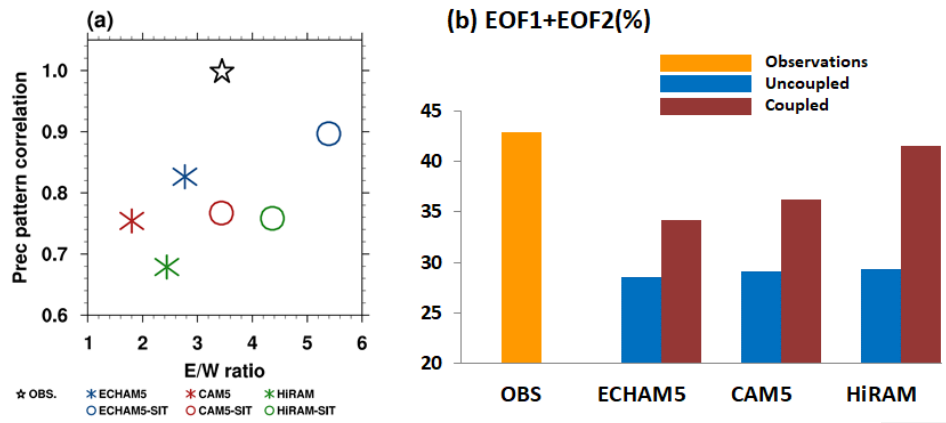
874

875 **Figure 6.** Vertical ocean temperature ($^{\circ}\text{C}$) profiles with respect to MJO phases for
 876 intraseasonal anomalies (i.e., with 20–100-day filtering) in observations and simulations
 877 using coupled models. Observations are in suit with data from TAO. Because of storage
 878 limitations, only 3 and 10 m water temperatures are presented in the HiRAM-SIT
 879 simulation.

880

881

882



883

884 **Figure 7.** Scatter plots of various MJO indices based on observation and experiments

← 格式化: 不要貼齊格線

885 (Table 1). (a) X-axis is the power ratio of east–west propagating waves. The east–west

886 ratio was calculated ~~through the division of by dividing~~ the sum ~~of~~ eastward-propagating

887 power by the westward-propagating counterpart within wavenumbers 1–3 (1–2 for zonal

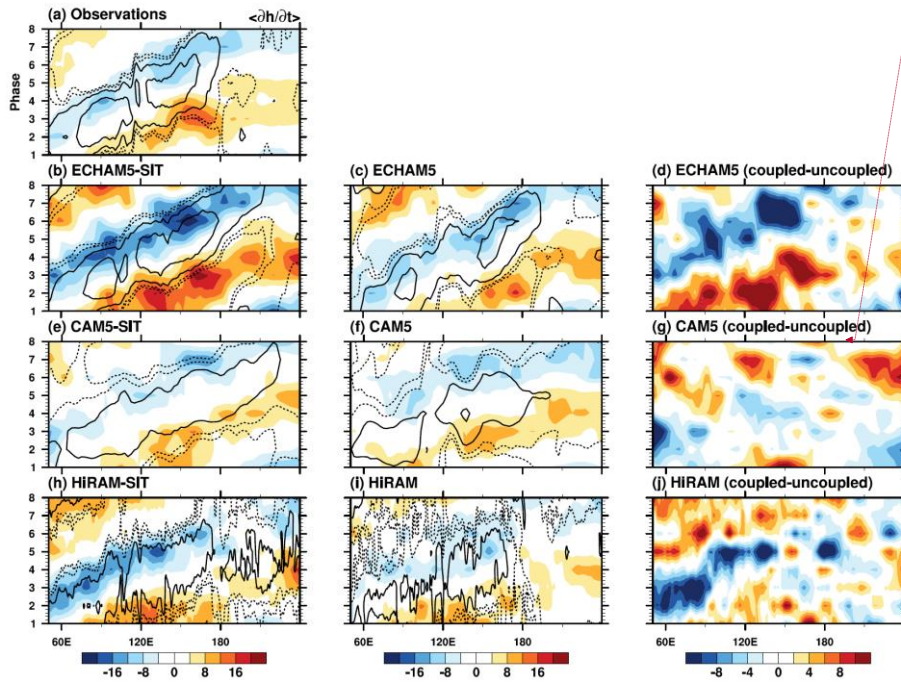
888 wind), period 30–80 days. ~~The~~ Y-axis is the pattern correlation of precipitation eastward

889 propagation, as shown in Fig. 2. (b) Sum of RMM1 and RMM2 variances based on

890 Wheeler and Hendon (2004).

891

892



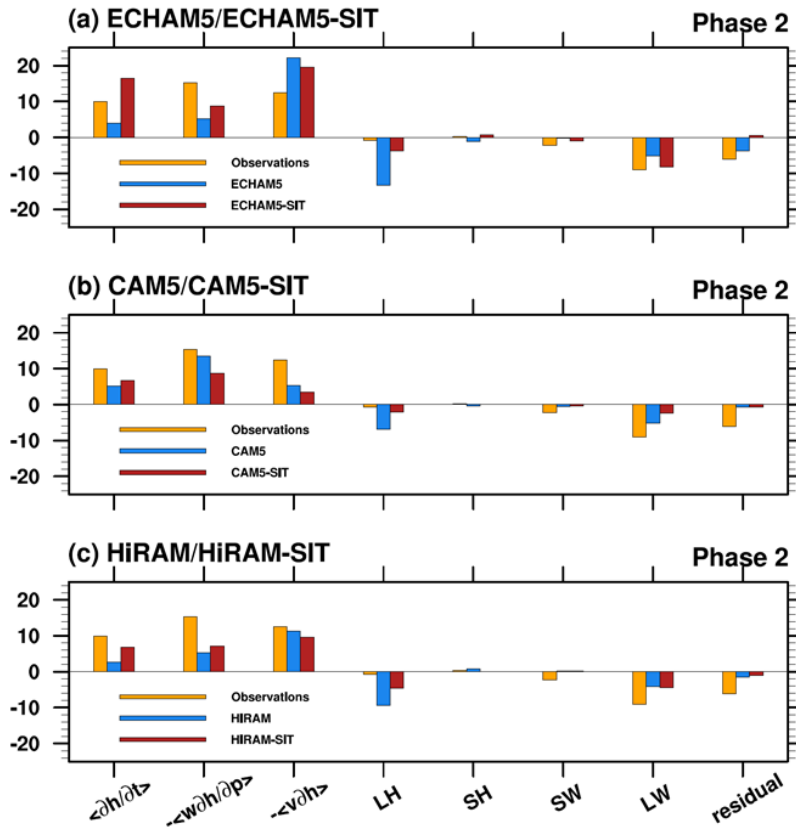
格式化: 不要貼齊格線

893

894 **Figure 6.** The 10°S -EQ averaged Hovmöller diagrams of MSE (shading: J kg^{-1}) and
 895 precipitation (contour: mm day^{-1}) composite followed the RMM index from (a)
 896 observations and simulations by using the (b, e, j) coupled and (c, f, k) uncoupled
 897 AGCMs and (d, i, l) their difference. The contour interval is precipitation
 898 anomalies.

格式化: 字型: 粗體

899



格式化: 不要貼齊格線

格式化: 字型色彩: 自動

格式化: 字型色彩: 自動

900

901 **Figure 79.** Model-simulated column-integrated MSE budget terms ($\text{J kg}^{-1} \text{s}^{-1}$) during
902 phase 2 of the MJO. ~~Data~~Black, red, and blue represents the data from the observations,

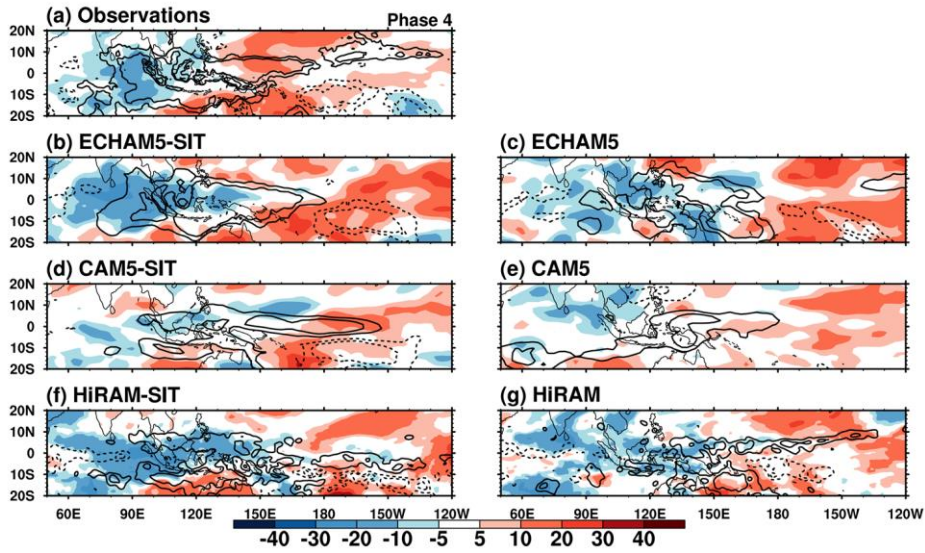
903 Nordeng scheme simulation, and Tiedtke scheme simulation-are shown in black, red, and

904 blue, respectively. The averaged domain is 10°S –EQ and 120° – 150°E .

905

906

907



908

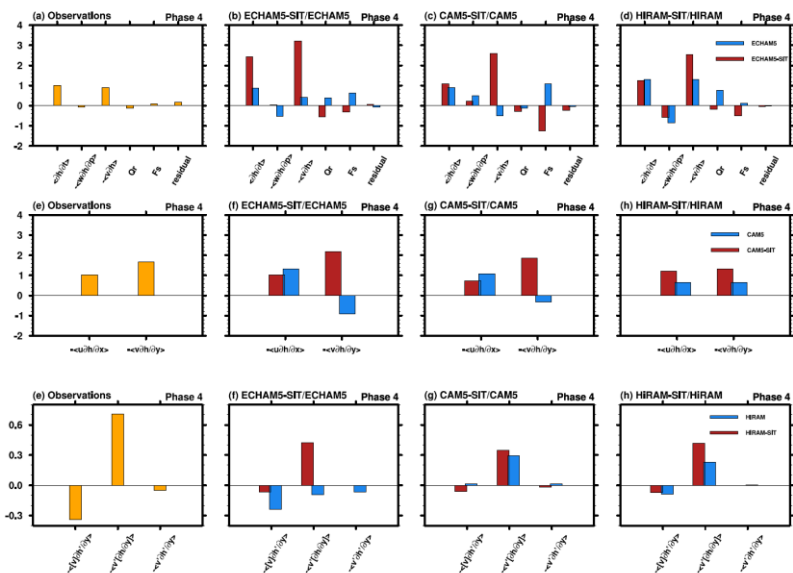
909 **Figure 810.** Phase 4 of the column-integrated MSE tendency (shading: $\text{J kg}^{-1} \text{s}^{-1}$) and
 910 precipitation (contours: mm day^{-1}) based on (a) observation, (b) ECHAM5-SIT, (c)
 911 ECHAM5, (d) CAM5-SIT, (e) CAM5, (g) HiRAM-SIT, and (f) HiRAM. The nine-point
 912 local smoothing is applied in the intraseasonal precipitation variance of HiRAM here
 913 (contours only).

914

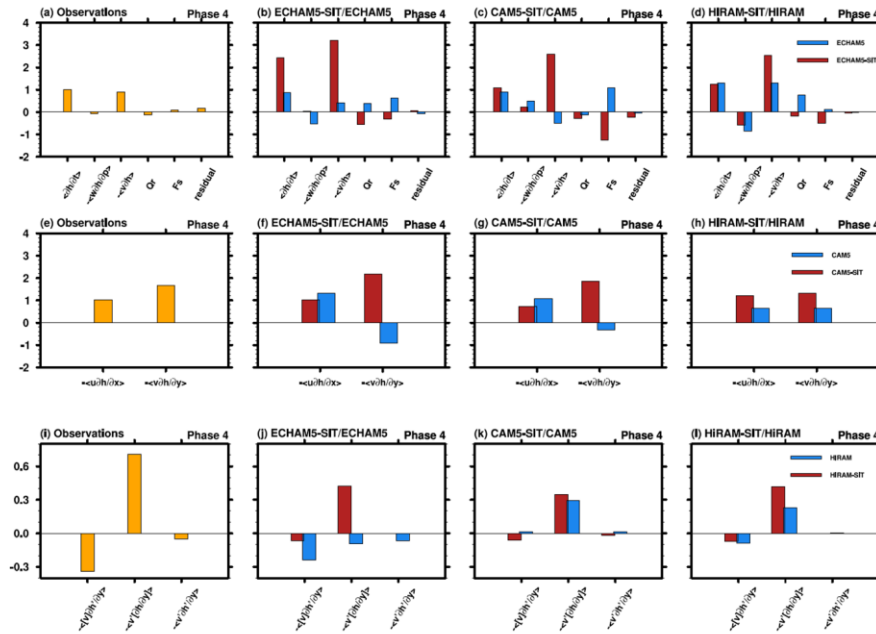
915

916

格式化: 不要貼齊格線



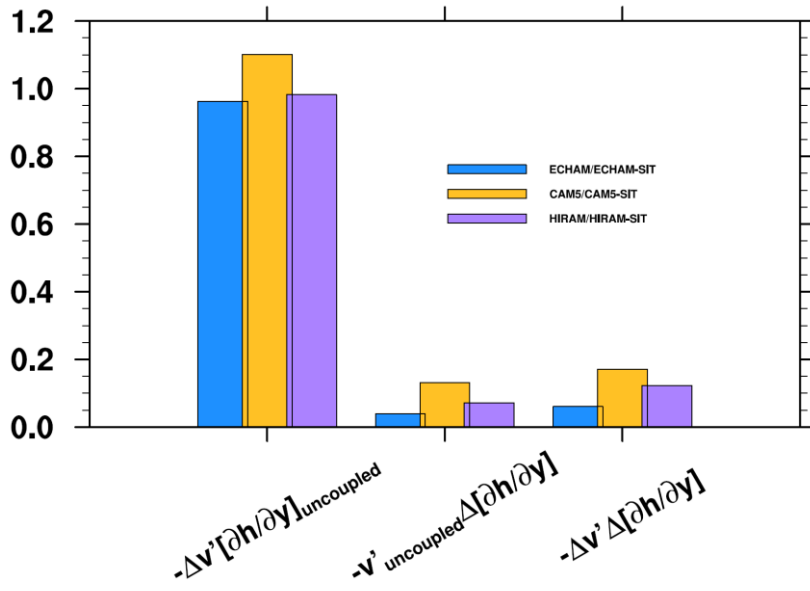
917



918

919 **Figure 911.** (a–d) Relative role of each MSE component of phase 4 through the projection
 920 of the spatial pattern of each MSE budget over the MC (domain) onto the total MSE
 921 tendency pattern (Fig. 8a). (e–h) Decompose of the total horizontal MSE advection
 922 based on zonal and meridional components. (i–l) Decompose of the meridional
 923 horizontal MSE advection based on the MJO circulation and the mean state of moisture.

924



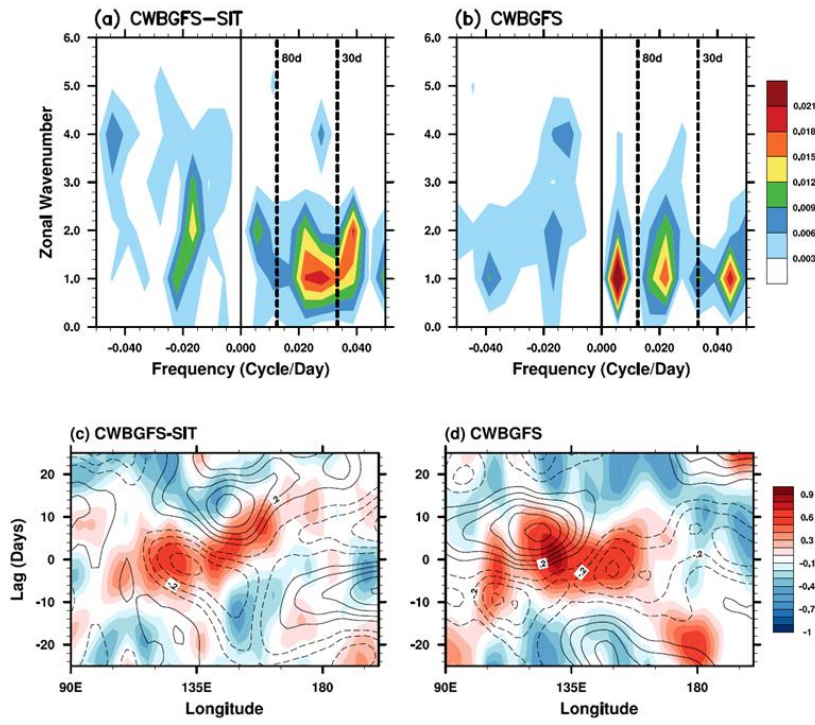
格式化: 不要貼齊格線

925

926 **Figure 1012.** Bar chart of relative contribution of intraseasonal convergence and
 927 background moisture between the coupled and uncoupled ~~changechanges~~ in MJO phase
 928 4.

929

930



931

932 **Figure 11.** (a, b) Same as Fig. 1, but in CWBGFS-SIT and CWBGFS. (c, d) Same as Fig.

933 2, but in CWBGFS-SIT and CWBGFS.

934

935

格式化: 行距: 2 倍行高, 不要贴齐格线